

# Detection of slow slip events along the southern Peru - northern Chile subduction zone

Jorge Jara<sup>1</sup>, Romain Jolivet<sup>2</sup>, Anne Socquet<sup>3</sup>, Diana Comte<sup>4</sup>, and Edmundo O. Norabuena<sup>5</sup>

<sup>1</sup>GFZ German Research Centre for Geosciences

<sup>2</sup>Ecole Normale Supérieure

<sup>3</sup>Université Grenoble Alpes

<sup>4</sup>Universidad de Chile

<sup>5</sup>Instituto Geofísico del Perú

May 11, 2023

# Detection of slow slip events along the southern Peru - northern Chile subduction zone

J. Jara \*, R. Jolivet <sup>1,2</sup>, A. Socquet <sup>3</sup>, D. Comte <sup>4,5</sup>, E. Norabuena <sup>6</sup>

<sup>1</sup>Laboratoire de Géologie, Département de Géosciences, École Normale Supérieure, PSL Research University, CNRS UMR 8538, Paris, France, <sup>2</sup>Institut Universitaire de France, Paris, France, <sup>3</sup>Université Grenoble Alpes, Université Savoie Mont Blanc, CNRS, IRD, IFSTTAR, ISTerre, Grenoble, France, <sup>4</sup>Departamento de Geofísica, Facultad de Ciencias Físicas y Matemáticas, Universidad de Chile, Blanco Encalada 2002, Santiago, Chile, <sup>5</sup>Advanced Mining Technology Center, Facultad de Ciencias Físicas y Matemáticas, Universidad de Chile, Av. Tupper 2007, Santiago, Chile, <sup>6</sup>Instituto Geofísico del Perú, Lima, Perú

Author contributions: *Conceptualization*: A. S., J. J. *Methodology*: J. J., R. J. *Formal Analysis*: J. J. *Investigation*: J. J. *Resources*: D. C., E. N. *Writing - original draft*: J. J. *Writing - Review & Editing*: J. J., R. J., A. S., D. C.

**Abstract** Detections of slow slip events (SSEs) are now common along most plate boundary fault systems at the global scale. However, no such event has been described in the south Peru - north Chile subduction zone so far, except for the early preparatory phase of the 2014 Iquique earthquake. We use geodetic template matching on GNSS-derived time series of surface motion in Northern Chile to extract SSEs hidden within the geodetic noise. We detect 33 events with durations ranging from 9 to 40 days and magnitudes from  $M_w$  5.6 to 6.2. The moment released by these aseismic events seems to scale with the cube of their duration, suggesting a dynamic comparable to that of earthquakes. We compare the distribution of SSEs with the distribution of coupling along the megathrust derived using Bayesian inference on GNSS- and InSAR-derived interseismic velocities. From this comparison, we obtain that most SSEs occur in regions of intermediate coupling where the megathrust transitions from locked to creeping or where geometrical complexities of the interplate region have been proposed. We finally discuss the potential role of fluids as a triggering mechanism for SSEs in the area.

**Non-technical summary** Earthquakes correspond to a sudden release of elastic energy stored in the crust as a response to the relative motion of tectonic plates. However, this release of energy is not always sudden and accompanied by destructive seismic waves. It sometimes happens slowly during aseismic, slow slip events. It has been shown that SSEs can be associated with the nucleation, propagation, and termination of big earthquakes. Therefore, it is crucial to develop systematized detection methods to characterize the physics governing aseismic slip. Here, we use a template matching method to scan GNSS observations of ground motion to detect and characterize slow slip events along southern Peru - northern Chile subduction zone where such events

\*Corresponding author: now at GFZ Potsdam, jorge@gfz-potsdam.de

have not been described previously. We find 33 SSEs at depths comparable with that of SSEs in other subduction zones, as well as in regions that slip aseismically persistently. We discuss how our findings relate to past earthquake ruptures, the geometry of the subduction zone, and fluids circulating at depth. Our results show the importance of implementing methods to extract small aseismic signals in noisy data, key observations for a better understanding of fault mechanics.

## 1 Introduction

Overwhelming evidence suggests that the Elastic Rebound Theory proposed by Reid (1910) after the 1906 California earthquake associated with the stick-slip behavior of frictional interface (Brace and Byerlee, 1966) is insufficient to explain the slip behavior along active faults. Geodetic measurements of surface motion have revealed and confirmed the presence of aseismic, slow slip along all types of active faults. After the first descriptions in the mid-20th century from direct observations of damage to human-made structures crossing the San Andreas (Louderback, 1942; Steinbrugge et al., 1960) and North Anatolian (Ambraseys, 1970) faults, aseismic slip has been directly observed, or inferred, from geodetic measurements at different stages of the earthquake cycle. For instance, afterslip corresponds to the diffusion of slow slip during the post-seismic period accommodating a co-seismic stress perturbation (e.g., Heki et al., 1997; Bürgmann et al., 2001; Hsu et al., 2002, 2006). Creep, on the other hand, often refers to steady aseismic slip during the interseismic period (Steinbrugge et al., 1960; Ambraseys, 1970; Jolivet et al., 2015b). In addition, interseismic transients (i.e., slow slip events or SSE) during this interseismic period were discovered in the 2000s along subduction zones. SSEs often locate in the deeper portion of the seismogenic zone (e.g., Hirose et al., 1999; Dragert et al., 2001), but some of these SSEs are associated with seismic signals that occur within the seismogenic zone, and may contribute to reducing geodetic coupling (Mazzotti et al., 2000; Bürgmann et al., 2005; Loveless and Meade, 2010; Radiguet et al., 2012; Béjar-Pizarro et al., 2013; Villegas-Lanza et al., 2016; Métois et al., 2016; Michel et al., 2019a; Jolivet et al., 2020; van Rijsingen et al., 2021). This along-dip segmentation differs from one subduction zone to the other (Nishikawa et al., 2019) and we note more occurrences of SSEs along young, warm subduction zones (i.e., Nankai, Mexico, Cascadia), than old and cold ones. Finally, slow slip appears to be an important ingredient of the preparation phase of earthquakes (e.g., Ruegg et al., 2001; Ruiz et al., 2014; Radiguet et al., 2016; Socquet et al., 2017; Voss et al., 2018). More recently, it has been proposed that a significant fraction of observed geodetic displacement in seismically active regions results from the occurrence of slow slip events (Jolivet and Frank, 2020, and reference therein), suggesting a burst-like, episodic behavior of aseismic slip at all time scales from seconds to decades in places as varied as Mexico (Frank, 2016; Rousset et al., 2017; Frank and Brodsky, 2019), Cascadia (Michel et al., 2019a; Ducellier et al., 2022; Itoh et al., 2022), along the San Andreas Fault (Khoshmanesh and Shirzaei, 2018; Rousset et al., 2019; Michel et al., 2022), the Haiyuan fault in Tibet (Jolivet et al., 2015a; Li et al., 2021), or Japan (Nishimura et al., 2013; Takagi et al., 2019; Nishikawa et al., 2019; Uchida et al., 2020). All observations suggest the importance of accounting for aseismic slip in our understanding of earthquake cycle dynamics. However, the underlying physics controlling aseismic slip is still debated, mainly due to the lack of good, dense observational databases.

Nowadays, observations of aseismic slip in subduction zones are frequently documented over a wide range of

slip amplitudes and at different stages of the earthquake cycle (Avouac, 2015; Obara and Kato, 2016; Bürgmann, 2018; Kato and Ben-Zion, 2021, and references therein). But regular slow slip events have been documented mainly along warm subduction zones such as Cascadia, Nankai (southwest Japan), Mexico, or New Zealand (e.g., Graham et al., 2016; Nishikawa et al., 2019; Wallace, 2020; Michel et al., 2022, and references therein). Instead, observations of slow slip events in cold subduction zones such as off-shore Japan or Chile are sparse or indirect, through seismic swarms, repeaters, or slow earthquakes (Kato et al., 2012; Kato and Nakagawa, 2014; Gardonio et al., 2018; Nishikawa et al., 2019), and rarely with geodetic observations (Hino et al., 2014; Ruiz et al., 2014; Socquet et al., 2017; Boudin et al., 2021). Geodetic displacement corresponding to such slow slip events are usually of mm to cm-scale amplitude and require the development of novel and systematized methods to extract SSEs from noisy time series of geodetic data (Frank, 2016; Rousset et al., 2017; Michel et al., 2019a; Uchida et al., 2020; Itoh et al., 2022).

We focus on the South Peru- North Chile subduction zone. The region is seismically active, with two historical earthquakes in 1868 (southern Peru), and 1877 (northern Chile), two tsunamigenic earthquakes of magnitude  $\sim 8.5$  (Kausel, 1986; Comte and Pardo, 1991; Vigny and Klein, 2022) (Figure 1). Since these two events, the region has experienced several large earthquakes ( $M_w > 7.5$ ) (Ruiz and Madariaga, 2018) accompanied by an important background seismic activity (Jara et al., 2017; Sippl et al., 2018, 2023) (Figure 1). In addition, coupling is highly variable along the subduction interface. Coupled regions overlap with the inferred rupture extent of the 2001  $M_w$  8.1 Arequipa and 2014  $M_w$  8.1 Iquique earthquakes (Schurr et al., 2014; Métois et al., 2016; Villegas-Lanza et al., 2016; Jolivet et al., 2020). A large coupled section is inferred where the 1877 earthquake is thought to have ruptured (Jolivet et al., 2020; Vigny and Klein, 2022). In addition, two low-coupling regions are observed. In southern Peru, low coupling coincides with the subduction of the Nazca ridge ( $\sim 15^\circ$ ) (Villegas-Lanza et al., 2016). In northern Chile, a reduction in coupling is inferred offshore Iquique and offshore the Mejillones peninsula ( $\sim 21^\circ$ ) (Béjar-Pizarro et al., 2013; Métois et al., 2016; Jolivet et al., 2020).

In addition to low coupling, aseismic slip has been observed in South Peru and North Chile. Afterslip has been reported following large earthquakes, including the 1995  $M_w$  8.1 Antofagasta (Chlieh et al., 2004; Pritchard and Simons, 2006), the 2001  $M_w$  8.1 Arequipa (Ruegg et al., 2001; Melbourne, 2002), the 2007  $M_w$  8.0 Pisco (Perfettini et al., 2010; Remy et al., 2016), the 2007  $M_w$  7.7 Tocopilla (Béjar-Pizarro et al., 2010) and the 2014  $M_w$  8.1 Iquique earthquakes (Hoffmann et al., 2018) (Figure 1). Geodetic transients interpreted as the signature of aseismic slip occurred in the days to months preceding the  $M_w$  8.4 Arequipa earthquake in 2001, before one of its largest aftershock, and preceding the Iquique earthquake in 2014 (e.g., Ruegg et al., 2001; Melbourne, 2002; Ruiz et al., 2014; Schurr et al., 2014; Socquet et al., 2017). Aseismic slip is considered responsible for a significant fraction of such geodetic transients (Twardzik et al., 2022). There is therefore plenty of evidence of occurrences of aseismic slip in this broad region but, despite intense efforts to instrument the area, no obvious spontaneous slow slip events have been detected during the interseismic period.

That said, a change in the interseismic surface velocity field was observed following the  $M_w$  7.5 intermediate-depth Tarapaca earthquake over a decade (Peyrat et al., 2006; Peyrat and Favreau, 2010) (Figure 1), an observation interpreted as the signature of a decoupling of the subduction interface (Ruiz et al., 2014; Jara et al., 2017). Over the same period, we observed a significant increase in background seismicity (Jara et al., 2017), as well as an apparent

synchronization of intermediate-depth and shallow seismic activities (Bouchon et al., 2016; Jara et al., 2017). Changes in background seismicity rates have been associated with the occurrence of aseismic slip events and fluid migration (Marsan et al., 2013; Reverso et al., 2016; Marsan et al., 2017). The synchronization of the seismicity is interpreted as related to aseismic slip events occurring along the subduction interface due to a broader slab deformation (Bouchon et al., 2016). These indirect observations suggest aseismic transients may occur in South Peru - North Chile during the interseismic period.

We aim to detect small, short-term aseismic slip events in this region and discuss their occurrence and location with respect to the interseismic coupling pattern and past seismic crises. We explore GNSS time series, searching for small transients, using a geodetic template matching approach (Rousset et al., 2017). We use GNSS and InSAR data to infer an updated distribution of interseismic coupling using a Bayesian framework following the approach of Jolivet et al. (2020), comparing the detected aseismic events with the coupling model, along with geophysical information available in the region (seismicity,  $V_p/V_s$  ratio, gravity models). We finally discuss potential mechanisms explaining the occurrence of aseismic events in the area.

## 2 Data, Methods and Results

### 2.1 GNSS processing and time series analysis

We process data from 119 continuous GNSS (cGNSS) sites in the central Andes region (Figure S1a) and worldwide (Figure S1b), using a double difference approach with the GAMIT/GLOBK software (Herring et al., 2015). 67 cGNSS sites are in the South Peru - North Chile region (Figure S1a and Figure 2, brown arrows), installed and maintained by the Integrate Plate boundary Observatory Chile (IPOC) (Klotz et al., 2017), the Laboratoire International Associé “Montessus de Ballore” (LIA-MB) (Klein et al., 2022), the Central Andean Tectonic Observatory (CAnTO, Caltech) (Simons et al., 2010), the Instituto Geofísico del Perú (IPG) (Jara et al., 2017; Socquet et al., 2017), the Institut des Sciences de la Terre (ISTerre) (Jara et al., 2017; Socquet et al., 2017), and the Centro Sismológico Nacional of Chile (CSN) (Báez et al., 2018). The remaining 52 stations are part of the International GNSS Service (IGS) (Teunissen and Montenbruck, 2017) global network. We separate these stations into three subnetworks (two locals and one global) with 33 overlapping stations, where the local separation depends on the station data span: one local network with data from 2000-2014 and the other including data from 2007-2014. Global network processing includes 99 stations over the 2000 - 2014 period, with 22 stations in South America (Figure S1b). We use the GAMIT 10.6 software (Herring et al., 2015), choosing ionosphere-free combinations and fixing the ambiguities to integer values. We use precise orbits from the IGS, precise earth-orientation parameters (EOPs) from the International Earth Rotation and Reference System Service (IERS) bulletin B, IGS tables to describe the phase centers of the antennas, FES2004 ocean-tidal loading corrections, and atmospheric loading corrections (tidal and non-tidal). We estimate one tropospheric zenith delay every two hours and one couple of horizontal tropospheric gradients per 24h session using the Vienna Mapping Function (VMF1) (Boehm et al., 2006). We use the GLOBK software to combine daily solutions and the PYACS software (Nocquet, 2018) to derive position time series in the ITRF 2008 reference frame (Altamimi et al., 2011). Finally, time series are referenced to fixed South-America considering the Euler pole solution proposed by Nocquet et al. (2014).

We fit the time series with a parametric function of time for each component (N, E, and U) (Bevis and Brown,

2014). Each time series  $x(t)$ , function of time  $t$ , writes as

$$x(t) = x_R + v(t - t_R) + \sum_{j=1}^{n_j} b_j H(t - t_j) + \sum_{k=1}^{n_F} [s_k \sin(\omega_k t) + c_k \cos(\omega_k t)] + \sum_{i=i}^{n_T} a_i \log(1 + t_i/\Delta T), \quad (1)$$

where  $x_R$  is a reference position at a time  $t_R$  and  $v$  is the interseismic velocity for each component.  $H$  is a Heaviside function applied each time  $t_j$  an earthquake (or antenna change) offset the time series. The combination of sin and cos functions describes seasonal oscillations (with annual and semi-annual periods), while the logarithmic function models the transient, post-seismic signal following large earthquakes ( $M_w \geq 7.5$ ) with a relaxation time  $\Delta T$ . For a given station, we consider a Heaviside function for all earthquakes of magnitude larger than 6 with an epicenter to station distance lower than  $d(M)_s = 10^{\frac{M}{2}-0.8}$ , as proposed by the Nevada Geodetic Laboratory ([www.geodesy.unr.edu](http://www.geodesy.unr.edu)). We only include a post-seismic term for earthquakes of magnitude larger than 7.5. All inferred parameters for each component and each cGPS site are in Supplementary Information, Tables S1-S38. Figures S2-S17 compare the data and model at each station. We then estimate and remove a common-mode by stacking all the time series (Bock and Melgar, 2016; Socquet et al., 2017; Jara et al., 2017). This procedure enables us to get residual time series (Figures S18-S19) as well as an interseismic velocity field (Table S1-S2). We use the obtained residual time series to search for geodetic transients compatible with slip on the megathrust and use the geodetic velocity field to update the last published coupling map (Jolivet et al., 2020).

## 2.2 Fault Geometry and Green's Functions

Coupling map estimation and geodetic template matching methods need a fault geometry and Green's functions calculation, as described below. In both cases, we define the geometry of the megathrust using Slab 2.0 (Hayes et al., 2018) as a reference, but with different meshing strategies. For the coupling case, we use 10 km-long sides triangles along the coast and 25 km-long sides, both at the trench and depth, between latitudes 17°S-25°S. In the northern part (10°S-17°S), we adapt the size to the GNSS station density, considering a constant 50 km-long triangle side. In contrast, in the geodetic template matching case, we use 10 km-long sides triangles along the coast and 25 km-long sides in the entire region. Then, we consider slip on the fault as the linear interpolation of slip values at the mesh nodes. Finally, we compute the Green's functions assuming a stratified elastic medium derived from Husen et al. (1999) using the EDKS software (Zhu and Rivera, 2002).

## 2.3 Coupling map for Southern Peru - Northern Chile

We update the distribution of coupling from Jolivet et al. (2020) in order to compare short- (i.e., days to months) and long-term (i.e., years to decades) aseismic deformation in the region. We use the GNSS velocity fields from Métois et al. (2016) and Villegas-Lanza et al. (2016), that we complement with our GNSS velocity field (Figure 2a). Additionally, we use the line of sight (LOS) velocity map from Jolivet et al. (2020), derived from the processing of Envisat data covering the period 2003 - 2010 (Figure 2b).

We use the backslip approach to estimate the distribution of coupling (Savage, 1983). A coupling of 1 (resp. 0) corresponds to a fully locked megathrust (resp. a megathrust that slips at plate rate). We consider plate motion esti-



mated by UNAVCO ([www.unavco.org](http://www.unavco.org)) under the ITRF 2014 model (Altamimi et al., 2016) to estimate the convergence rate, angle, and rake on each node of the fault mesh. The backslip rate is evaluated by subtracting the sliver movement proposed by Métois et al. (2016) in Chile (11 mm/yr) and by (Villegas-Lanza et al., 2016) in Peru (5.5 mm/yr) to the convergence rate. In the Arica bend (16°S - 18°S), at the boundary of the Chilean and Peruvian slivers, we build a gradient to make a smooth transition between the two slivers. We solve for the distribution of models that satisfy the geodetic data.

The forward problem writes as  $\mathbf{d} = \mathbf{G}\mathbf{m}$ , with  $\mathbf{d}$  the geodetic data (GNSS and InSAR velocities),  $\mathbf{m}$  the vector of parameters to solve for and  $\mathbf{G}$  the Green's functions (Section 2.2). Parameters include coupling at each mesh node and geometric transformations akin to those in Jolivet et al. (2020). We adopt a probabilistic approach to estimate the parameters in order to evaluate the associated uncertainties. The *a posteriori* Probability Density Function (PDF) of a model  $\mathbf{m}$  given a dataset  $\mathbf{d}$ ,  $p(\mathbf{m}|\mathbf{d})$ , writes as

$$p(\mathbf{m}|\mathbf{d}) \propto p(\mathbf{m})p(\mathbf{d}|\mathbf{m}), \quad (2)$$

where  $p(\mathbf{m})$  is the *a priori* model PDF and  $p(\mathbf{d}|\mathbf{m})$  is the data likelihood. The *a priori* PDF describes our knowledge of coupling along the megathrust before collecting geodetic data. The *a priori* PDF at each node for the coupling factor is a Gaussian distribution centered on 0 bounded by -0.1 and 1.1. We know the megathrust is decoupled below 60 km depth based on geodetic (Chlieh et al., 2004; Béjar-Pizarro et al., 2013; Jolivet et al., 2020), and seismological evidence (Comte et al., 2016). Thus, we apply an *a priori* constraint depending on the depth of each node. If deeper than 60 km, the standard deviation of the *a priori* PDF of coupling for a node is 0.1. If shallower than 60 km, we set the standard deviation of the *a priori* PDF to 5. In our *a priori*, coupling is relatively unknown at depths shallower than 60 km and constrained to lower values otherwise.

We adopt a Gaussian formulation for the data likelihood, which writes as,

$$p(\mathbf{d}|\mathbf{m}) = \frac{1}{\sqrt{2}\mathbf{C}_\chi} \exp\left\{-\frac{1}{2}(\mathbf{G}\mathbf{m} - \mathbf{d})^T \mathbf{C}_\chi^{-1}(\mathbf{G}\mathbf{m} - \mathbf{d})\right\}, \quad (3)$$

where  $\mathbf{C}_\chi$  is the misfit covariance matrix (Duputel et al., 2014) defined as  $\mathbf{C}_\chi = \mathbf{C}_p + \mathbf{C}_d$ , where  $\mathbf{C}_d$  is the data covariance matrix (data uncertainties), while  $\mathbf{C}_p$  is the prediction error covariance matrix, representing uncertainties on the assumed elastic model (P and S wave velocities and density). We assume a 10% error on the elastic parameters following Jolivet et al. (2020).

We explore the model space using Altar ([altar.readthedocs.io](http://altar.readthedocs.io)) to sample the *a posteriori* PDF of the coupling factor, generating 250000 models. Altar is based on the Cascading Adaptive Transitional Metropolis in Parallel (CATMIP) algorithm (Minson et al., 2013; Duputel et al., 2014; Jolivet et al., 2015b). These models enable us to perform statistics, derive the mean model for the interseismic coupling (Figure 3), and collect information about the model resolution (see Supporting Information for model GNSS and InSAR residuals, Figure S20-S23, as well as Standard Deviation, Mode, Skewness, and Kurtosis, Figure S24).

The mean coupling model (Figure 3a), is close to previously published models in the region (e.g., Chlieh et al., 2011; Béjar-Pizarro et al., 2013; Métois et al., 2016; Villegas-Lanza et al., 2016; Jolivet et al., 2020), especially considering the

along-strike segmentation. Our model differs from previously published models in the coupling intensity at locked patches, as well as the depth of these coupled patches. In Peru, we observe three patches with interseismic coupling that varies between 0.5-0.75 (Figure 3a). Previous models report similar patches, although totally locked (coupling factor  $\sim 1$ ) (Chlieh et al., 2011; Villegas-Lanza et al., 2016). Unfortunately, the density of GNSS stations in this region is not anywhere near that in Chile, hence the large standard deviations in the Peruvian region (Figure S25). Analyzing the moments of the *a posteriori* PDF, including standard deviation, skewness and kurtosis confirms this (Figure S24). Similarly, these moments show that the resolution at the trench over the entire region is low. Additionally, our model varies from those constrained only by GPS data in Chile (e.g., Métois et al., 2016). The InSAR data helps constraining interseismic coupling at depth (Béjar-Pizarro et al., 2013; Jolivet et al., 2020) and the strong *a priori* coupling damps potential large variations at depth, which we consider not physical.

## 2.4 Detection of aseismic slip events with geodetic template matching

### 2.4.1 Methodology

We use a geodetic template matching approach to detect potential aseismic slip events on the residual GNSS time series (Section 2.1). We summarize here the method presented in detail by Rousset et al. (2019). We search for the spatio-temporal signature of slip events in surface displacement time series by cross-correlating synthetic templates with our GNSS residual time series, in velocity. These templates correspond to the surface displacement caused by slip on dislocations located on the subduction megathrust embedded in a stratified, semi-infinite elastic medium. We calculate such templates ( $\mathbf{w}$ ) by convolving the Green's functions (Section 2.2) with a time-dependent slip evolution  $\mathbf{s}(t)$  defined as

$$\mathbf{s}(t) = \frac{1}{2} \left[ 1 - \cos \left( \frac{\pi t}{T} \right) \right], \quad (4)$$

where  $T$  is the duration of a synthetic event. Following Rousset et al. (2019), we derive for each template the weighted correlation function for each fault node, defined as

$$\mathbf{C}_f(t) = \frac{\sum_{i=1}^{2N} |\mathbf{G}_i| \mathbf{C}_i(t)}{\sum_{i=1}^{2N} |\mathbf{G}_i|}, \quad (5)$$

where  $\mathbf{G}$  denotes the Green's functions and  $\mathbf{C}_i$  is the correlation between the time series and the synthetic template at a given fault node  $i$  given by

$$\mathbf{C}_i(t) = \frac{\sum_{k=1}^T \dot{\mathbf{w}}_i(t_k) \dot{\mathbf{d}}_i(t_k + \tau)}{\sqrt{\sum_{k=1}^T \dot{\mathbf{w}}_i^2(t_k) \sum_{k=1}^T \dot{\mathbf{d}}_i^2(t_k + \tau)}}, \quad (6)$$

where  $\mathbf{w}$  denotes the template of a given length  $T$ ,  $\mathbf{d}$  are the displacement time series, and  $\tau$  is a moving temporal variable. We search for peaks in  $\mathbf{C}_f(t)$  corresponding to candidate slip events (see Supporting Information for a synthetic example in Figure S31).

For each candidate slip event, we stack the time series of displacement weighted by Green's functions around the



time of detection. Such weighting accounts for displacement amplitude and direction, increasing the signal-to-noise ratio (Rousset et al., 2017). Stacks are computed over a period of 80 days, centered on each potential occurrence. On each stack, we estimate two linear trends, before and after the candidate occurrence, and the time dependent slip evolution of Eq. 4 to the weighted stack in order to determine the amplitude, the start and end date of each detected transient. We apply a non-linear regression to determine the posterior Probability Density Function of the model parameters given a stack of time series following Tarantola (2005). Effectively, we use an MCMC algorithm to derive 30,000 samples from the posterior PDF and evaluate the mean and standard deviation of the duration and magnitude of each candidate slow slip event.

In order to curate the potential detections from artefacts, we perform a sensitivity and resolution analysis, to determine the minimum magnitude of a slip event that can be detected for each fault node. Although the method above has been extensively described by Rousset et al. (2019), the novelty of our approach relies on the evaluation of uncertainties through a Bayesian exploration of all important parameters.

#### 2.4.2 GNSS network sensitivity and resolution

We analyze the sensitivity of our approach by testing its ability to detect, locate, and estimate the source parameters (magnitude and duration) of synthetic aseismic slip events. We first evaluate the parameters characterizing the noise affecting each GNSS time series of displacement by building synthetic time series of noise on which we perform the tests. In order to generate synthetic noise, we model each component of the residual time series (Eq. 1) as a combination of white and colored noise (Williams, 2003), such as,

$$\mathbf{P}(f) = P_0 (\mathbf{f}^{-\alpha} + f_0^{-\alpha}), \quad (7)$$

where  $\mathbf{P}$  is the power spectrum as function of temporal frequency  $\mathbf{f}$ ,  $P_0$  and  $f_0$  are normalization constants, and  $\alpha$  is the spectral index. We explore  $P_0$ ,  $f_0$ , and  $\alpha$  using Bayesian inference to estimate their mean and standard deviation at each station component (see the Supporting Information for further details and an example of the power spectrum and the probability density function (PDF) of parameters at the UAPE station in Figures S26 - S27, as well as Tables S39 - S42 for all the network noise parameters inferred). We use these inferred noise parameters to build 1000 synthetic time series of displacement at each GNSS station. We use these synthetic time series to estimate thresholds of detection for each fault node.

The number of GNSS stations in the study area has evolved during the observation period. We, therefore, must consider three periods independently depending on the number of active stations: 2000 - 2003 (four stations), 2004 - 2007 (20 stations), and 2008 - 2014 (55 stations). We first determine which stations are able to capture a slow slip event on a given node. For each period and fault node, we correlate the 1000 synthetic time series of noise with a template of a duration of 40 days and slip equivalent to a magnitude  $M_w$  6.0. We evaluate the standard deviation of the resulting weighted correlation functions,  $\sigma_t$ , as a minimal threshold to be exceeded (i.e., when dealing with time series that might include slip events, a peak of correlation higher than  $3\sigma_t$  is a positive detection).

Once this threshold has been defined, we compute the weighted correlation function for 1000 time series of noise to which we have added the signal of synthetic transients with different duration (10, 20, and 30 days) and magnitudes

(5.0 - 7.0  $M_w$ , every 0.1 of magnitude). In case of a detection, we stack the displacement time series around the detection time. We consider a synthetic event has been correctly detected and located if we can recover four quantities, including the slip event location, timing, duration, and magnitude. If the estimated location is within 150 km from the true location, if the estimated timing and duration are within five days of the actual ones, and if the estimated magnitude is within 0.25 of the actual one, we consider the detection to be valid. This procedure enables us to determine the minimum magnitude that can be detected over each of the three observation periods and build resolution maps for each period investigated (see Supporting Information, Figures S29-S30). For instance, in the Iquique region ( $\sim 19^\circ\text{S} - 71^\circ\text{W}$ ), the minimal magnitude  $M_w$  varies from 6.8-6.6 in 2000-2003, decreasing to 6.3-6.1 in 2004-2007, and arriving to 6.1-5.9 in 2008-2014. Thus, as expected, we observe a significant improvement in detection sensitivity when the number of stations in the region increases.

## 2.5 Application to GNSS time series

After exploring the network sensitivity to detect aseismic slip events, we search for transients in the residual time series obtained after subtracting the trajectory model described earlier. We fix the duration  $T$  of the template to 40 days and the slip to an event equivalent to  $M_w$  6.0. By doing so, we detect 733 candidate slip events in the stacked correlation functions. Since some of these candidates may correspond to the same candidate slip event, we retain maximum occurrences within a radius of 150 km (i.e., if two maxima affect nodes separated by a distance higher than 150 km, they are considered as independent occurrences). After this selection step, we are left with 59 candidate slip events in the region. We evaluate their durations and magnitudes and compare these with our resolution maps. We keep candidates for which the obtained magnitude are higher than the minimum detectable magnitude for the corresponding node (Figure 4), leaving us with 33 validated slip events.

The duration of the slip events ranges from 9 to 40 days with magnitudes from  $M_w$  5.6 to 6.2 and depths from 20 to 66 km. Figure 3 shows the location of the detected slip events along with four examples of weighted stacks. Figure 5 shows two examples of stack, along with the time series used to build the stacks (see Supplementary information Tables S43 for the event parameters estimated with their uncertainties, and Figures S33 - S40 to see the data employed in the modeling, the data stack, and the model).

Since the template matching approach only considers GNSS observations, we must ensure that the detected slip events are mostly aseismic. We cross-check the 33 positive detections with the seismic catalog provided by the ISC (International Seismological Centre, 2016). We randomly generate 10000 synthetic locations for each slip event considering a normally distributed location uncertainty based on our resolution tests and estimate the sum of the seismic moment of all earthquakes occurring within at least a  $2\sigma$  radius of the detected slip event. We then compare this estimate of the seismic moment to the estimated aseismic one. All the detected slip events have an equivalent magnitude at least twice larger than the seismic magnitude (aseismic/seismic ratio for each event and further details on ratio estimation are in Supplementary Information, Table S43). Figures 5 (c) and (f) present the location of the two events detailed in Figure 5 (a) and (c) together with the seismicity that coincides with the occurrence of the slip event. These two events occur during the preparation (Events #16) and postseismic (Event #8) phases of the 2014 Iquique earthquake (Figure 1). The combination of synthetic tests and the seismic vs. aseismic moment analysis confirms we detected 33 aseismic slip events along southern Peru - northern Chile subduction zone over the period 2006 - 2014.

### 3 Discussion

#### 3.1 Aseismic slip events and scaling laws

Aseismic slip events are now frequently observed along most subduction zones in the world, but the underlying physics is still debated. Among the points of debate, the comparison between slow slip and earthquakes should allow to point out whether comparable physics are involved. [Ide et al. \(2007\)](#) have proposed that, while the seismic moment of earthquakes is proportional to the cube of their duration, the moment of slow earthquakes, from tremors and low-frequency earthquakes to slow slip events, is proportional to the duration. Considering that simple considerations about size and stress drop led to the emergence of the observed scaling for earthquakes, the difference in moment-duration scaling should involve a fundamental difference between the mechanics of slow slip and that of earthquakes. [Peng and Gomberg \(2010\)](#) argued that the apparent moment duration scaling of slow earthquakes proposed by [Ide et al. \(2007\)](#) was only due to a lack of observations, suggesting both rapid and slow slip were driven by the same mechanism, namely a slip instability with variable speed and stress drop propagating along a weakened fault surface. In addition, [Gomberg et al. \(2016\)](#) proposed that seismic moment scales either with the duration or the cube of the duration depending on whether the rupture was elongated and pulse-like or mostly crack-like. [Michel et al. \(2019b\)](#) confirmed that the moment of slow slip events in Cascadia scales with the cube of their duration although being elongated and pulse-like. These observations agree with recent studies of aseismic slip and tremors in Japan ([Takagi et al., 2019](#); [Supino et al., 2020](#)) and Mexico ([Frank and Brodsky, 2019](#)), as well as numerical modeling using dynamic simulations of frictional sliding ([Dal Zilio et al., 2020](#)). Such numerical and observational evidence suggests that SSEs might exhibit comparable scaling as classical earthquakes, only with lower rupture speeds and stress drops.

We evaluate the scaling between moment and duration for the aseismic slip events we have detected. We estimate that the moment,  $M$ , is such as  $M \propto T^{3.11 \pm 0.01}$  with  $T$  the duration, in agreement with [Michel et al. \(2019b\)](#) in Cascadia (Figure 6, and Figure S42). Following the scheme proposed by [Gomberg et al. \(2016\)](#), we infer that the rupture velocity of our detected events ranges between 0.5 and 10 km/day with a stress drop of 0.1 MPa. Although our method does not allow to detect events that would propagate, the scaling we observe suggests our slow slip events are more compatible with crack-like, unbounded ruptures than pulse-like, bounded ones. Therefore, observations point towards a cubic scaling for slow slip events along southern Peru - northern Chile region.

#### 3.2 Aseismic slip and interseismic coupling distribution

Our coupling estimate corresponds to an average behavior over a decade, without accounting for potential slow slip events hidden within the noise. The slow slip events we detect correspond to fluctuations around this average. We compare the map of coupling to the location of our 33 aseismic events to explore how such fluctuations distribute with respect to locked and creeping asperities along the megathrust (Figure 3). We compare the distribution of coupling where our events are located to a distribution coupling at randomly picked locations (Figure 7). The distributions differ but mostly when considering only events in northern Chile, where our estimate of coupling is much more robust. Detected slow slip events occur mostly in regions of intermediate coupling. This observation is not as clear for the Peruvian region, probably because of the sparsity of the data used here, although the same tendency is suggested on Figure 7. Events offshore Peru tend to cluster spatially around locked asperities, in areas of intermediate coupling

(Figure 8). In general, slow slip events occur in transitional regions between seismic asperities and freely slipping areas. This is consistent with model predictions from rate-and-state friction in which slow slip events are expected to occur at the transition between seismic, rate-weakening and creeping, rate-strengthening asperities (e.g., [Liu and Rice, 2005, 2007](#); [Perfettini and Ampuero, 2008](#)).

The average depth of the detected slow slip events is 35 km (Figure 7). Separating the events yields an average depth of 37 km for Peru and 33.5 km for northern Chile with comparable standard deviations (17 and 12 km respectively, Figure 7). [Lay \(2015\)](#) separates the subduction megathrust along depth into four domains (A, B, C, and D). Domain A, located between the trench and a depth of about 15 km, hosts either tsunami earthquakes or aseismic deformation. Domain B, between approximately 15 and 30 km depth, hosts large megathrust earthquakes. Domain C, between approximately 30 and 50 km depth, hosts intermediate sized earthquakes. At greater depths, Domain D, between 50 and 70 km, hosts slow slip events, tremors, and very low-frequency earthquakes. Our slow slip events mainly occur in Domains C and D. It is understood that small, velocity weakening asperities in Domain C are embedded in conditionally stable regions of the megathrust, prone to host slow slip events. Domain D is dominated by aseismic sliding and potential slip rate variations could explain deeper detections. Therefore, the depth distribution of our events matches regions where slow slip events are expected in a subduction zone context.

Our resolution tests (Figures S24, S29-S30) suggest that it is impossible to capture aseismic slip near the trench, in domain A, with the current GNSS network. However, large, shallow slow slip events have been observed in Japan ([Nishimura, 2014](#); [Nishikawa et al., 2019](#)) and New Zealand ([Wallace, 2020](#)). Seafloor geodesy might help to detect the occurrence of such large events and potentially for small, cm-scale ones comparable to our aseismic slip events ([Araki et al., 2017](#)). Additionally, stress-shadow induces apparent coupling in velocity-weakening regions, especially late in the interseismic period ([Hetland and Simons, 2010](#); [Lindsey et al., 2021](#)). For this reason, we also cannot rule out the potential occurrence of aseismic slip event near the trench.

In addition to the depth-dependent segmentation, we observe an along-strike segmentation in the distribution of SSEs. In particular, we observe a lack of events within the rupture area of the 1877 earthquake, within the Arequipa rupture area and other detections gather around locked asperities, like in the doughnut model for seismicity ([Kanamori, 1981](#); [Schurr et al., 2020](#)). Such configuration is comparable to that of the Japan trench where the asperity that ruptured during the Tohoku earthquake in 2011 overwhelms the simple depth-dependent distribution of behavior from [Lay \(2015\)](#). In particular, [Nishikawa et al. \(2019\)](#) propose that, unlike the Nankai subduction interface which exhibits a depth-dependent segmentation due to a young, warm slab, the megathrust beneath Tohoku is not segmented at depth into four distinct domains. In our area of interest, the subducting slab is older than the Nankai slab and probably colder ([Müller et al., 2008](#)), which would explain why the behavior we unravel is not completely consistent with that of [Lay \(2015\)](#) and potentially closer to that of the Japan trench.

As an additional level of complexity, three events coincide with the subduction of the Nazca ridge (14°S, Figures 3 and 8a), eight events are located beneath the Mejillones Peninsula (23°S, Figures 3 and 8d), and four events are within the Arica bend (17°S - 19°S, Figures 3 and 8b and c). These morphological structures are anomalies compared to the model proposed by [Lay \(2015\)](#) as they are considered as barriers to the propagation of large earthquakes ([Armijo and Thiele, 1990](#); [Comte and Pardo, 1991](#); [Béjar-Pizarro et al., 2010](#); [Villegas-Lanza et al., 2016](#)). In these regions, the depth

of our detected slow slip event does not match the depth-dependency described by [Lay \(2015\)](#). We can speculate that local geometrical complexities may lead to the occurrence of slow slip events ([Romanet et al., 2018](#)) in the case of the subduction of the Nazca Ridge or that the apparent low coupling is the result of multiple slow slip events ([Jolivet et al., 2020](#)) in the case of the Arica Bend.

### 3.3 Aseismic slip events before and after large earthquakes

Among all the detected slow slip events, only events #8, #16, and #31 (Figure 3) do not occur during the steady inter-seismic period. Event #8 locates in the region struck by the Iquique earthquake in 2014 (Figure 8c) during the post-seismic relaxation that followed the mainshock ([Meng et al., 2015](#); [Hoffmann et al., 2018](#); [Shrivastava et al., 2019](#)) ( $M_w$  5.9 and duration of 18 days in June 2014). Event #31 is detected during the post-seismic phase of the Tocopilla earthquake in 2007 (Figure 1,  $M_w$  5.8 and duration of 25 days in February 2008). Although afterslip does not seem to extend further than one month after the mainshock ([Béjar-Pizarro et al., 2010](#); [Motagh et al., 2010](#)), the timing of event #31 ( $\sim 2$  months after the earthquake) and its location at the northern end of the mainshock ([Motagh et al., 2010](#); [Schurr et al., 2012](#)) suggest that stress redistribution caused by significant afterslip could have led to its occurrence. Such slow slip events embedded within a post-seismic sequence have already been observed following the Illapel earthquake ([Tissandier et al., 2023](#)) and in a completely different setting, following the 2004 Parkfield earthquake, along the San Andreas Fault ([Michel et al., 2022](#)).

Aseismic slip has been recognized as an important element of the earthquake preparation phase ([Obara and Kato, 2016](#); [McLaskey, 2019](#); [Kato and Ben-Zion, 2021](#), and references therein). An 8-month-long slow slip event was reported before the Iquique earthquake in 2014 ([Socquet et al., 2017](#)), and event #16 coincides with one of the regions of the megathrust that slipped aseismically during that preparation phase (Figure 8 c). In addition, event #16 occurred where and when intermediate-depth and shallow seismicity synchronized before the Iquique earthquake ([Bouchon et al., 2016](#); [Jara et al., 2017](#)) ( $M_w$  6.0 and duration of 21 days in January 2014). Such synchronization of seismicity began in January 2014, lasted for one month, and is interpreted as evidence of a slow, slab-wide deformation process prior to megathrust earthquakes ([Bouchon et al., 2016](#)). Furthermore, event #16 is coincident with the transient event reported by [Boudin et al. \(2021\)](#) using a long-base tiltmeter. Our epicentral location differs by 50km from the one reported by ([Boudin et al., 2021](#)), a difference that can be explained by different modeling strategies and/or uncertainties. We propose that event #16 is linked to the 8-month aseismic slip transient observed preceding the 2014 Iquique earthquake. Such detection suggests the growing instability preceding the Iquique earthquake exhibits a complex spatio-temporal behavior that hides within the noise of the data, in agreement with the hypothesis proposed by [Jolivet and Frank \(2020\)](#).

### 3.4 Aseismic slip and fluids

Fluids may also play a role in the occurrence of aseismic slip events ([Avouac, 2015](#); [Harris, 2017](#); [Jolivet and Frank, 2020](#), and references therein). Pore pressure affects fault normal stress, hence modify the probability of a slip instability as well as the nucleation size ([Liu and Rice, 2007](#); [Avouac, 2015](#); [Bayart et al., 2016](#); [Harris, 2017](#); [Bürgmann, 2018](#); [Jolivet and Frank, 2020](#); [Behr and Bürgmann, 2021](#)). An increase in pore pressure within the fault zone leads to a decrease in normal stress, which promotes slip but increases nucleation size, promoting slow slip. We compare



our detections to the distribution of the  $V_p/V_s$  ratio and to gravity-inferred structural models in the region. We use the  $V_p/V_s$  ratio inferred by Comte et al. (2016) for the events located in Northern Chile. Statistically, the 21 aseismic events in northern Chile are not related to a specific  $V_p/V_s$  value (Fig. 7). In particular, no slow slip events are found to collocate with high  $V_p/V_s$  ratios ( $V_p/V_s > 1.8$ ) (Comte et al., 2016).

We also compare the location of our aseismic events to a 3-D density model in the region (Tassara and Echaurren, 2012). Figure 9 shows the location of aseismic events along ten different trench-perpendicular cross sections. The slow slip events are primarily located along the contact between the slab and the overriding lithospheric mantle (Figure 9). This mantle corner is principally hydrated by the dehydration of the subducting slab due to water releasing metamorphic reactions (Peacock, 2001; Rüpke et al., 2004; Comte et al., 2016; Contreras-Reyes et al., 2021). Such reactions occur from depths of 30 to 100 km, and the fluids released might migrate along the subduction interface (Wang et al., 2019; Contreras-Reyes et al., 2021). The fact that our aseismic slip events tend to cluster at depths corresponding to the lithospheric mantle along the megathrust, and not deeper, might imply that fluids may be trapped and accumulate below the continental Moho, an hypothesis that would require further investigations.

## 4 Conclusions

We have systematically analyzed GNSS time series in the region, searching for the occurrence of aseismic slip events with a template matching approach. We find 33 events in the period 2006 - 2014, with durations of 9 - 40 days, magnitudes of  $M_w$  5.6 - 6.2, and located at depths of 20-66 km. These events are mostly aseismic and are observed at all stages of the earthquake cycle, including during post-seismic periods (afterslip, two events), earthquake preparation phase (one event), and interseismic period (30 events). We compare those slow slip occurrence to a wide range of possible models of interseismic coupling based on GNSS and InSAR velocity fields and infer a distribution of coupling along the megathrust.

We propose that in the region, the seismic moment of detected events scale to the cube of their duration, advocating for comparable physics underlying slow slip events and earthquakes. We do not find particular correlations with published seismic velocity structures but find that slow slip events cluster around past ruptures and locked asperities, where the megathrust transitions from sliding to locked. Additionally, our events are located in regions of intermediate coupling values and mean depths of 35 km, which match regions where slow slip events occur in the context of subduction zones.

Some of these events occur on the subduction interface deeper than than the continental MOHO, i.e. where the slab is in contact with the mantle wedge corner where fluids are supposedly trapped. This points toward the influence of fluids is the triggering of the slow slip event, as it may explain both their spontaneous triggering and their long duration. However, as some events are found at shallower depth, the involvement of fluids might not be the only explanation. Other mechanisms such as geometrical complexities might be involved but more evidence are required.

The main outcome of this study is that we found numerous aseismic slip events in a place where none were found during the interseismic period before. As a consequence, aseismic slip events may be found elsewhere in subduction zone contexts where experts did not find any event, pending dedicated noise analysis methods. We provide here one



piece of evidence supporting the hypothesis proposed by Jolivet and Frank (2020) which states that slow slip happens everywhere and at all times.

## Acknowledgements

The authors thank the Laboratoire International Associé “Montessus de Ballore” (LIA-MB), International Plate Boundary Observatory Chile (IPOC, [www.ipoc-network.org](http://www.ipoc-network.org)), Central Andean Tectonic Observatory Geodetic Array (CAnTO, [www.tectonics.caltech.edu/resources/continuous\\_gps.html](http://www.tectonics.caltech.edu/resources/continuous_gps.html)), and Instituto Geofísico del Perú ([www.igp.gob.pe](http://www.igp.gob.pe)) for making the raw GNSS data available, as well as all researchers, technicians, and students involved in the installation and maintenance of such networks. J. Jara acknowledges a PhD scholarship granted by Chilean National Science Cooperation (CONICYT) through “Becas Chile” Program. A. Socquet and J. Jara benefited from a grant from ANR (ANR-17-CE31-0002-01, project AtypicSSE). J. Jara, R. Jolivet and A. Socquet acknowledge the funding of the European Research Council (ERC) under the European Union’s Horizon 2020 research and innovation program (grant agreement 758210, project Geo4D and grant agreement 865963, project DEEPtrigger). R. Jolivet acknowledges funding from the Institut Universitaire de France. D. Comte acknowledges the funding provided by ANID via the projects PIA/ANID grant ACT-192169, and ANID Project AFB180004, AFB220002. The authors would like to thank J. Pina-Valdes, H. Bhat, H. Sanchez-Reyes, S. Michel, C. Vigny, R. Madariaga, and M. Bouchon for all the constructive discussions about this work.

## Data and code availability

GNSS time series used in this work can be found at: <https://doi.org/10.5281/zenodo.7898656>.

## References

- Altamimi, Z., Collilieux, X., and Métivier, L. ITRF2008: An improved solution of the international terrestrial reference frame. *Journal of Geodesy*, 85(8):457–473, 2011. doi: 10.1007/s00190-011-0444-4.
- Altamimi, Z., Rebischung, P., Métivier, L., and Collilieux, X. ITRF2014: A new release of the International Terrestrial Reference Frame modeling nonlinear station motions. *Journal of Geophysical Research: Solid Earth*, 121(8):6109–6131, 2016. doi: 10.1002/2016JB013098.
- Ambraseys, N. Some characteristic features of the Anatolian fault zone. *Tectonophysics*, 9(2-3):143–165, 3 1970. doi: 10.1016/0040-1951(70)90014-4.
- Araki, E., Saffer, D. M., Kopf, A. J., Wallace, L. M., Kimura, T., Machida, Y., Ide, S., and Davis, E. Recurring and triggered slow-slip events near the trench at the Nankai Trough subduction megathrust. *Science*, 356(6343):1157–1160, 2017. doi: 10.1126/science.aan3120.
- Armijo, R. and Thiele, R. Active faulting in northern Chile: ramp stacking and lateral decoupling along a subduction plate boundary? *Earth and Planetary Science Letters*, 98(1):40–61, 4 1990. doi: 10.1016/0012-821X(90)90087-E.
- Avouac, J.-P. From Geodetic Imaging of Seismic and Aseismic Fault Slip to Dynamic Modeling of the Seismic Cycle. *Annual Review of Earth and Planetary Sciences*, 43(1):233–271, 2015. doi: 10.1146/annurev-earth-060614-105302.
- Báez, J. C., Leyton, F., Troncoso, C., del Campo, F., Bevis, M., Vigny, C., Moreno, M., Simons, M., Kendrick, E., Parra, H., and Blume, F. The Chilean GNSS Network: Current Status and Progress toward Early Warning Applications. *Seismological Research Letters*, 89(4):1546–1554, 7 2018. doi: 10.1785/0220180011.

- Bayart, E., Svetlizky, I., and Fineberg, J. Slippery but Tough: The Rapid Fracture of Lubricated Frictional Interfaces. *Physical Review Letters*, 116(19):194301, 5 2016. doi: 10.1103/PhysRevLett.116.194301.
- Beck, S. L. and Ruff, L. J. Great earthquakes and subduction along the Peru trench. *Physics of the Earth and Planetary Interiors*, 57(3-4): 199–224, 11 1989. doi: 10.1016/0031-9201(89)90112-X.
- Behr, W. M. and Bürgmann, R. What's down there? The structures, materials and environment of deep-seated slow slip and tremor. *Philosophical Transactions of the Royal Society A: Mathematical, Physical and Engineering Sciences*, 379(2193):20200218, 3 2021. doi: 10.1098/rsta.2020.0218.
- Béjar-Pizarro, M., Carrizo, D., Socquet, A., Armijo, R., Barrientos, S., Bondoux, F., Bonvalot, S., Campos, J., Comte, D., De Chabaliér, J. B., and others. Asperities and barriers on the seismogenic zone in North Chile: state-of-the-art after the 2007 Mw 7.7 Tocopilla earthquake inferred by GPS and InSAR data. *Geophysical Journal International*, 183(1):390–406, 2010. doi: 10.1111/j.1365-246X.2010.04748.x.
- Béjar-Pizarro, M., Socquet, A., Armijo, R., Carrizo, D., Genrich, J., and Simons, M. Andean structural control on interseismic coupling in the North Chile subduction zone. *Nature Geoscience*, 6(6):462–467, 6 2013. doi: 10.1038/ngeo1802.
- Bevis, M. and Brown, A. Trajectory models and reference frames for crustal motion geodesy. *Journal of Geodesy*, 88(3):283–311, 3 2014. doi: 10.1007/s00190-013-0685-5.
- Bock, Y. and Melgar, D. Physical applications of GPS geodesy: A review. *Reports on Progress in Physics*, 79(10):106801, 2016. doi: 10.1088/0034-4885/79/10/106801.
- Boehm, J., Werl, B., and Schuh, H. Troposphere mapping functions for GPS and very long baseline interferometry from European Centre for Medium-Range Weather Forecasts operational analysis data. *Journal of Geophysical Research: Solid Earth*, 111(2), 2006. doi: 10.1029/2005JB003629.
- Bouchon, M., Marsan, D., Durand, V., Campillo, M., Perfettini, H., Madariaga, R., and Gardonio, B. Potential slab deformation and plunge prior to the Tohoku, Iquique and Maule earthquakes. *Nature Geoscience*, 9(5):380–383, 5 2016. doi: 10.1038/ngeo2701.
- Boudin, F., Bernard, P., Meneses, G., Vigny, C., Olcay, M., Tassara, C., Boy, J. P., Aissaoui, E., Métois, M., Satriano, C., Esnault, M.-F., Nercessian, A., Vallée, M., Vilotte, J.-P., and Brunet, C. Slow slip events precursory to the 2014 Iquique Earthquake, revisited with long-base tilt and GPS records. *Geophysical Journal International*, 228(3):2092–2121, 2021. doi: 10.1093/gji/ggab425.
- Brace, W. F. and Byerlee, J. D. Stick-Slip as a Mechanism for Earthquakes. *Science*, 153(3739):990–992, 8 1966. doi: 10.1126/science.153.3739.990.
- Bürgmann, R. The geophysics, geology and mechanics of slow fault slip. *Earth and Planetary Science Letters*, 495:112–134, 2018. doi: 10.1016/j.epsl.2018.04.062.
- Bürgmann, R., Kogan, M. G., Levin, V. E., Scholz, C. H., King, R. W., and Steblov, G. M. Rapid aseismic moment release following the 5 December, 1997 Kronotsky, Kamchatka, earthquake. *Geophysical Research Letters*, 28(7):1331–1334, 4 2001. doi: 10.1029/2000GL012350.
- Bürgmann, R., Kogan, M. G., Steblov, G. M., Hilley, G., Levin, V. E., and Apel, E. Interseismic coupling and asperity distribution along the Kamchatka subduction zone. *Journal of Geophysical Research: Solid Earth*, 110(7):1–17, 2005. doi: 10.1029/2005JB003648.
- Chlieh, M., De Chabaliér, J. B., Ruegg, J. C., Armijo, R., Dmowska, R., Campos, J., and Feigl, K. L. Crustal deformation and fault slip during the seismic cycle in the North Chile subduction zone, from GPS and InSAR observations. *Geophysical Journal International*, 158(2):695–711, 2004. doi: 10.1111/j.1365-246X.2004.02326.x.
- Chlieh, M., Perfettini, H., Tavera, H., Avouac, J. P., Remy, D., Nocquet, J. M., Rolandone, F., Bondoux, F., Gabalda, G., and Bonvalot, S. Interseismic coupling and seismic potential along the Central Andes subduction zone. *Journal of Geophysical Research: Solid Earth*, 116 (12), 2011. doi: 10.1029/2010JB008166.

- Comte, D. and Pardo, M. Reappraisal of great historical earthquakes in the northern Chile and southern Peru seismic gaps. *Natural Hazards*, 4(1):23–44, 1991. doi: 10.1007/BF00126557.
- Comte, D., Carrizo, D., Roecker, S., Ortega-Culaciati, F., and Peyrat, S. Three-dimensional elastic wave speeds in the northern Chile subduction zone: Variations in hydration in the supraslab mantle. *Geophysical Journal International*, 207(2):1080–1105, 2016. doi: 10.1093/gji/ggw318.
- Contreras-Reyes, E., Díaz, D., Bello-González, J. P., Slezak, K., Potin, B., Comte, D., Maksymowicz, A., Ruiz, J. A., Osses, A., and Ruiz, S. Subduction zone fluids and arc magmas conducted by lithospheric deformed regions beneath the central Andes. *Scientific Reports*, 11(1):1–12, 2021. doi: 10.1038/s41598-021-02430-9.
- Dal Zilio, L., Lapusta, N., and Avouac, J. P. Unraveling Scaling Properties of Slow-Slip Events. *Geophysical Research Letters*, 47(10), 2020. doi: 10.1029/2020GL087477.
- Delouis, B., Monfret, T., Dorbath, L., Pardo, M., Rivera, L., Comte, D., Haessler, H., Caminade, J. P., Ponce, L., Kausel, E., and Cisternas, A. The Mw= 8.0 antofagasta (northern Chile) earthquake of 30 July 1995: A precursor to the end of the large 1877 gap. *Bulletin of the Seismological Society of America*, 87(2):427–445, 1997.
- Dorbath, L., Cisternas, A., and Dorbath, C. Assessment of the size of large and great historical earthquakes in Peru. *Bulletin of the Seismological Society of America*, 80(3):551–576, 1990.
- Dragert, H., Wang, K., and James, T. S. A Silent Slip Event on the Deeper Cascadia Subduction Interface. *Science*, 292(5521):1525–1528, 5 2001. doi: 10.1126/science.1060152.
- Ducellier, A., Creager, K. C., and Schmidt, D. A. Detection of Slow Slip Events Using Wavelet Analysis of GNSS Recordings. *Bulletin of the Seismological Society of America*, 112(5):2408–2424, 2022. doi: 10.1785/0120210289.
- Duputel, Z., Agram, P. S., Simons, M., Minson, S. E., and Beck, J. L. Accounting for prediction uncertainty when inferring subsurface fault slip. *Geophysical Journal International*, 197(1):464–482, 4 2014. doi: 10.1093/gji/ggt517.
- Duputel, Z., Jiang, J., Jolivet, R., Simons, M., Rivera, L., Ampuero, J. P., Riel, B., Owen, S. E., Moore, A. W., Samsonov, S. V., Ortega Culaciati, F., and Minson, S. E. The Iquique earthquake sequence of April 2014: Bayesian modeling accounting for prediction uncertainty. *Geophysical Research Letters*, 42(19):7949–7957, 2015. doi: 10.1002/2015GL065402.
- Dziewonski, A. M., Chou, T.-A., and Woodhouse, J. H. Determination of earthquake source parameters from waveform data for studies of global and regional seismicity. *Journal of Geophysical Research: Solid Earth*, 86(B4):2825–2852, 4 1981. doi: 10.1029/JB086iB04p02825.
- Ekström, G., Nettles, M., and Dziewoński, A. The global CMT project 2004–2010: Centroid-moment tensors for 13,017 earthquakes. *Physics of the Earth and Planetary Interiors*, 200-201:1–9, 6 2012. doi: 10.1016/j.pepi.2012.04.002.
- Frank, W. B. Slow slip hidden in the noise: The intermittence of tectonic release. *Geophysical Research Letters*, 43(19):125–10, 2016. doi: 10.1002/2016GL069537.
- Frank, W. B. and Brodsky, E. E. Daily measurement of slow slip from low-frequency earthquakes is consistent with ordinary earthquake scaling. *Science Advances*, 5(10):eaaw9386, 10 2019. doi: 10.1126/sciadv.aaw9386.
- Gardonio, B., Marsan, D., Socquet, A., Bouchon, M., Jara, J., Sun, Q., Cotte, N., and Campillo, M. Revisiting Slow Slip Events Occurrence in Boso Peninsula, Japan, Combining GPS Data and Repeating Earthquakes Analysis. *Journal of Geophysical Research: Solid Earth*, 123(2): 1502–1515, 2 2018. doi: 10.1002/2017JB014469.
- Gomberg, J., Wech, A., Creager, K., Obara, K., and Agnew, D. Reconsidering earthquake scaling. *Geophysical Research Letters*, 43(12): 6243–6251, 6 2016. doi: 10.1002/2016GL069967.
- Graham, S., DeMets, C., Cabral-Cano, E., Kostoglodov, V., Rousset, B., Walpersdorf, A., Cotte, N., Lasserre, C., McCaffrey, R., and Salazar-

- 566 Tlaczani, L. Slow Slip History for the MEXICO Subduction Zone: 2005 Through 2011. *Pure and Applied Geophysics*, 173(10-11):3445–3465,  
567 2016. doi: 10.1007/s00024-015-1211-x.
- 568 Harris, R. A. Large earthquakes and creeping faults. *Reviews of Geophysics*, 55(1):169–198, 2017. doi: 10.1002/2016RG000539.
- 569 Hartzell, S. and Langer, C. Importance of model parameterization in finite fault inversions: application to the 1974 MW 8.0 Peru earthquake.  
570 *Journal of Geophysical Research*, 98(B12), 1993. doi: 10.1029/93jb02453.
- 571 Hayes, G. P., Moore, G. L., Portner, D. E., Hearne, M., Flamme, H., Furtney, M., and Smoczyk, G. M. Slab2, a comprehensive subduction zone  
572 geometry model. *Science*, 362(6410):58–61, 10 2018. doi: 10.1126/science.aat4723.
- 573 Heki, K., Miyazaki, S., and Tsuji, H. Silent fault slip following an interplate thrust earthquake at the Japan Trench. *Nature*, 386(6625):595–598,  
574 4 1997. doi: 10.1038/386595a0.
- 575 Herring, T. A., King, R., Floyd, M., and McClusky, S. C. GAMIT Reference Manual. GPS Analysis at MIT GLOBK, Release 10.6, 2015.
- 576 Hetland, E. A. and Simons, M. Post-seismic and interseismic fault creep II: Transient creep and interseismic stress shadows on megathrusts.  
577 *Geophysical Journal International*, 181(1):99–112, 2010. doi: 10.1111/j.1365-246X.2009.04482.x.
- 578 Hino, R., Inazu, D., Ohta, Y., Ito, Y., Suzuki, S., Iinuma, T., Osada, Y., Kido, M., Fujimoto, H., and Kaneda, Y. Was the 2011 Tohoku-Oki earthquake  
579 preceded by aseismic preslip? Examination of seafloor vertical deformation data near the epicenter. *Marine Geophysical Research*, 35  
580 (3):181–190, 2014. doi: 10.1007/s11001-013-9208-2.
- 581 Hirose, H., Hirahara, K., Kimata, F., Fujii, N., and Miyazaki, S. A slow thrust slip event following the two 1996 Hyuganada Earthquakes  
582 beneath the Bungo Channel, southwest Japan. *Geophysical Research Letters*, 26(21):3237–3240, 11 1999. doi: 10.1029/1999GL010999.
- 583 Hoffmann, F., Metzger, S., Moreno, M., Deng, Z., Sippl, C., Ortega-Culaciati, F., and Oncken, O. Characterizing Afterslip and Ground Displace-  
584 ment Rate Increase Following the 2014 Iquique-Pisagua Mw8.1 Earthquake, Northern Chile. *Journal of Geophysical Research: Solid Earth*,  
585 123(5):4171–4192, 5 2018. doi: 10.1002/2017JB014970.
- 586 Hsu, Y.-J., Bechor, N., Segall, P., Yu, S.-B., Kuo, L.-C., and Ma, K.-F. Rapid afterslip following the 1999 Chi-Chi, Taiwan Earthquake. *Geophysical*  
587 *Research Letters*, 29(16):1–4, 8 2002. doi: 10.1029/2002GL014967.
- 588 Hsu, Y. J., Simons, M., Avouac, J. P., Galetka, J., Sieh, K., Chlieh, M., Natawidjaja, D., Prawirodirdjo, L., and Bock, Y. Frictional afterslip  
589 following the 2005 Nias-Simeulue earthquake, Sumatra. *Science*, 312(5782):1921–1926, 2006. doi: 10.1126/science.1126960.
- 590 Husen, S., Kissling, E., Flueh, E., and Asch, G. Accurate hypocentre determination in the seismogenic zone of the subducting Nazca Plate  
591 in northern Chile using a combined on-/offshore network. *Geophysical Journal International*, 138(3):687–701, 1999. doi: 10.1046/j.1365-  
592 246X.1999.00893.x.
- 593 Ide, S., Beroza, G. C., Shelly, D. R., and Uchide, T. A scaling law for slow earthquakes. *Nature*, 447(7140):76–79, 2007. doi: 10.1038/na-  
594 ture05780.
- 595 International Seismological Centre. On-line Bulletin, 2016.
- 596 Itoh, Y., Aoki, Y., and Fukuda, J. Imaging evolution of Cascadia slow-slip event using high-rate GPS. *Scientific Reports*, 12(1):1–12, 2022.  
597 doi: 10.1038/s41598-022-10957-8.
- 598 Jara, J., Socquet, A., Marsan, D., and Bouchon, M. Long-Term Interactions Between Intermediate Depth and Shallow Seismicity in North  
599 Chile Subduction Zone. *Geophysical Research Letters*, 44(18):9283–9292, 9 2017. doi: 10.1002/2017GL075029.
- 600 Jara, J., Sánchez-Reyes, H., Socquet, A., Cotton, F., Virieux, J., Maksymowicz, A., Díaz-Mojica, J., Walpersdorf, A., Ruiz, J., Cotte, N., and  
601 Norabuena, E. Kinematic study of Iquique 2014 M w 8.1 earthquake: Understanding the segmentation of the seismogenic zone. *Earth*  
602 *and Planetary Science Letters*, 503:131–143, 2018. doi: 10.1016/j.epsl.2018.09.025.
- 603 Jolivet, R. and Frank, W. B. The Transient and Intermittent Nature of Slow Slip. *AGU Advances*, 1(1), 2020. doi: 10.1029/2019av000126.

- Jolivet, R. and Simons, M. A Multipixel Time Series Analysis Method Accounting for Ground Motion, Atmospheric Noise, and Orbital Errors. *Geophysical Research Letters*, 45(4):1814–1824, 2018. doi: 10.1002/2017GL076533.
- Jolivet, R., Candela, T., Lasserre, C., Renard, F., Klinger, Y., and Doin, M. The Burst-Like Behavior of Aseismic Slip on a Rough Fault: The Creeping Section of the Haiyuan Fault, China. *Bulletin of the Seismological Society of America*, 105(1):480–488, 2015a. doi: 10.1785/0120140237.
- Jolivet, R., Simons, M., Agram, P. S., Duputel, Z., and Shen, Z. K. Aseismic slip and seismogenic coupling along the central San Andreas Fault. *Geophysical Research Letters*, 42(2):297–306, 2015b. doi: 10.1002/2014GL062222.
- Jolivet, R., Simons, M., Duputel, Z., Olive, J. A., Bhat, H. S., and Bletery, Q. Interseismic Loading of Subduction Megathrust Drives Long-Term Uplift in Northern Chile. *Geophysical Research Letters*, 47(8):1–11, 2020. doi: 10.1029/2019GL085377.
- Kanamori, H. The Nature of Seismicity Patterns Before Large Earthquakes. In *Earthquake Prediction*, pages 1–19. Wiley Online Library, 3 1981. doi: 10.1029/ME004p0001.
- Kato, A. and Ben-Zion, Y. The generation of large earthquakes. *Nature Reviews Earth & Environment*, 2(1):26–39, 1 2021. doi: 10.1038/s43017-020-00108-w.
- Kato, A. and Nakagawa, S. Multiple slow-slip events during a foreshock sequence of the 2014 Iquique, Chile Mw 8.1 earthquake. *Geophysical Research Letters*, 41(15):5420–5427, 2014. doi: 10.1002/2014GL061138.
- Kato, A., Obara, K., Igarashi, T., Tsuruoka, H., Nakagawa, S., and Hirata, N. Propagation of slow slip leading up to the 2011 Mw9.0 Tohoku-Oki earthquake. *Science*, 335(6069):705–708, 2 2012. doi: 10.1126/science.1215141.
- Kausel, E. Los terremotos de agosto de 1868 y mayo de 1877 que afectaron el sur del Perú y norte de Chile. *Boletín de la Academia Chilena de Ciencias*, 3(1):8–13, 1986.
- Khoshmanesh, M. and Shirzaei, M. Episodic creep events on the San Andreas Fault caused by pore pressure variations. *Nature Geoscience*, 11(8):610–614, 2018. doi: 10.1038/s41561-018-0160-2.
- Klein, E., Vigny, C., Nocquet, J. M., and Boulze, H. A 20 year-long GNSS solution across South-America with focus in Chile. *BSGF - Earth Sciences Bulletin*, 193, 2022. doi: 10.1051/bsgf/2022005.
- Klotz, J., Deng, Z., Moreno, M., Asch, G., Bartsch, M., and Ramatschi, M. IPOC cGPS - Continuous Mode GPS data in the IPOC Region, Northern Chile. Technical report, GFZ Data Services, 2017.
- Lay, T. The surge of great earthquakes from 2004 to 2014. *Earth and Planetary Science Letters*, 409(October 2016):133–146, 2015. doi: 10.1016/j.epsl.2014.10.047.
- Li, Y., Nocquet, J. M., Shan, X., and Song, X. Geodetic Observations of Shallow Creep on the Laohushan-Haiyuan Fault, Northeastern Tibet. *Journal of Geophysical Research: Solid Earth*, 126(6):1–18, 2021. doi: 10.1029/2020JB021576.
- Lindsey, E. O., Mallick, R., Hubbard, J. A., Bradley, K. E., Almeida, R. V., Moore, J. D. P., Bürgmann, R., and Hill, E. M. Slip rate deficit and earthquake potential on shallow megathrusts. *Nature Geoscience*, 14(5):321–326, 5 2021. doi: 10.1038/s41561-021-00736-x.
- Liu, Y. and Rice, J. R. Aseismic slip transients emerge spontaneously in three-dimensional rate and state modeling of subduction earthquake sequences. *Journal of Geophysical Research: Solid Earth*, 110(8):1–14, 2005. doi: 10.1029/2004JB003424.
- Liu, Y. and Rice, J. R. Spontaneous and triggered aseismic deformation transients in a subduction fault model. *Journal of Geophysical Research: Solid Earth*, 112(9), 2007. doi: 10.1029/2007JB004930.
- Louderback, G. Faults and Earthquakes. *Bulletin of Seismological Society of America*, 32(4):305–330, 1942.
- Loveless, J. P. and Meade, B. J. Geodetic imaging of plate motions, slip rates, and partitioning of deformation in Japan. *Journal of Geophysical Research*, 115(B2):B02410, 2010. doi: 10.1029/2008JB006248.

- Marsan, D., Reverso, T., Helmstetter, A., and Enescu, B. Slow slip and aseismic deformation episodes associated with the subducting Pacific plate offshore Japan, revealed by changes in seismicity. *Journal of Geophysical Research E: Planets*, 118(9):4900–4909, 2013. doi: 10.1002/jgrb.50323.
- Marsan, D., Bouchon, M., Gardonio, B., Perfettini, H., Socquet, A., and Enescu, B. Change in seismicity along the Japan trench, 1990–2011, and its relationship with seismic coupling. *Journal of Geophysical Research: Solid Earth*, 122(6):4645–4659, 6 2017. doi: 10.1002/2016JB013715.
- Mazzotti, S. S., Le Pichon, X., Henry, P., and Miyazaki, S.-I. Full interseismic locking of the Nankai and Japan-west Kurile subduction zones: An analysis of uniform elastic strain accumulation in Japan constrained by permanent GPS. *Journal of Geophysical Research: Solid Earth*, 105(B6):13159–13177, 2000. doi: 10.1029/2000jb900060.
- McLaskey, G. C. Earthquake Initiation From Laboratory Observations and Implications for Foreshocks. *Journal of Geophysical Research: Solid Earth*, 124(12):12882–12904, 2019. doi: 10.1029/2019JB018363.
- Melbourne, T. I. Precursory transient slip during the 2001  $M_w = 8.4$  Peru earthquake sequence from continuous GPS. *Geophysical Research Letters*, 29(21):2032, 2002. doi: 10.1029/2002GL015533.
- Meng, L., Huang, H., Bürgmann, R., Ampuero, J. P., and Strader, A. Dual megathrust slip behaviors of the 2014 Iquique earthquake sequence. *Earth and Planetary Science Letters*, 411:177–187, 2015. doi: 10.1016/j.epsl.2014.11.041.
- Métois, M., Vigny, C., and Socquet, A. Interseismic Coupling, Megathrust Earthquakes and Seismic Swarms Along the Chilean Subduction Zone ( $38^\circ$ – $18^\circ$ S). *Pure and Applied Geophysics*, 173(5):1431–1449, 2016. doi: 10.1007/s00024-016-1280-5.
- Michel, S., Gualandi, A., and Avouac, J. P. Interseismic Coupling and Slow Slip Events on the Cascadia Megathrust. *Pure and Applied Geophysics*, 176(9):3867–3891, 2019a. doi: 10.1007/s00024-018-1991-x.
- Michel, S., Gualandi, A., and Avouac, J.-P. Similar scaling laws for earthquakes and Cascadia slow-slip events. *Nature*, 574(7779):522–526, 10 2019b. doi: 10.1038/s41586-019-1673-6.
- Michel, S., Jolivet, R., Lengliné, O., Gualandi, A., Larochelle, S., and Gardonio, B. Searching for Transient Slow Slips Along the San Andreas Fault Near Parkfield Using Independent Component Analysis. *Journal of Geophysical Research: Solid Earth*, 127(6):1–19, 2022. doi: 10.1029/2021JB023201.
- Minson, S. E., Simons, M., and Beck, J. L. Bayesian inversion for finite fault earthquake source models I-theory and algorithm. *Geophysical Journal International*, 194(3):1701–1726, 2013. doi: 10.1093/gji/ggt180.
- Motagh, M., Schurr, B., Anderssohn, J., Cailleau, B., Walter, T. R., Wang, R., and Villotte, J. P. Subduction earthquake deformation associated with 14 November 2007,  $M_w$  7.8 Tocopilla earthquake in Chile: Results from InSAR and aftershocks. *Tectonophysics*, 490(1-2):60–68, 2010. doi: 10.1016/j.tecto.2010.04.033.
- Müller, R. D., Sdrolias, M., Gaina, C., and Roest, W. R. Age, spreading rates, and spreading asymmetry of the world's ocean crust. *Geochimistry, Geophysics, Geosystems*, 9(4), 4 2008. doi: 10.1029/2007GC001743.
- Nishikawa, T., Matsuzawa, T., Ohta, K., Uchida, N., Nishimura, T., and Ide, S. The slow earthquake spectrum in the Japan Trench illuminated by the S-net seafloor observatories. *Science*, 365(6455):808–813, 2019. doi: 10.1126/science.aax5618.
- Nishimura, T. Short-term slow slip events along the Ryukyu Trench, southwestern Japan, observed by continuous GNSS. *Progress in Earth and Planetary Science*, 1(1):1–13, 2014. doi: 10.1186/s40645-014-0022-5.
- Nishimura, T., Matsuzawa, T., and Obara, K. Detection of short-term slow slip events along the Nankai Trough, southwest Japan, using GNSS data. *Journal of Geophysical Research: Solid Earth*, 118(6):3112–3125, 2013. doi: 10.1002/jgrb.50222.
- Nocquet, J. M. PYACS: A set of Python tools for GPS analysis and tectonic modelling. In *PYACS: A set of Python tools for GPS analysis and*



- 680 *tectonic modelling*. 19th General Assembly of Wegener, 2018.
- 681 Nocquet, J. M., Villegas-Lanza, J. C., Chlieh, M., Mothes, P. A., Rolandone, F., Jarrin, P., Cisneros, D., Alvarado, A., Audin, L., Bondoux, F.,  
682 Martin, X., Font, Y., Régnier, M., Vallée, M., Tran, T., Beauval, C., Maguiña Mendoza, J. M., Martinez, W., Tavera, H., and Yepes, H. Motion of  
683 continental slivers and creeping subduction in the northern Andes. *Nature Geoscience*, 7(4):287–291, 2014. doi: 10.1038/ngeo2099.
- 684 Obara, K. and Kato, A. Connecting slow earthquakes to huge earthquakes. *Science (New York, N.Y.)*, 353(6296):253–257, 2016.  
685 doi: 10.1126/science.aaf1512.
- 686 Peacock, S. M. Are the lower planes of double seismic zones caused by serpentine dehydration in subducting oceanic mantle? *Geology*, 29  
687 (4):299–302, 2001. doi: 10.1130/0091-7613(2001)029<0299:ATLPOD>2.0.CO;2.
- 688 Peng, Z. and Gomberg, J. An integrated perspective of the continuum between earthquakes and slow-slip phenomena. *Nature Geoscience*,  
689 3(9):599–607, 2010. doi: 10.1038/ngeo940.
- 690 Perfettini, H. and Ampuero, J. P. Dynamics of a velocity strengthening fault region: Implications for slow earthquakes and postseismic slip.  
691 *Journal of Geophysical Research: Solid Earth*, 113(9), 2008. doi: 10.1029/2007JB005398.
- 692 Perfettini, H., Avouac, J. P., Tavera, H., Kositsky, A., Nocquet, J. M., Bondoux, F., Chlieh, M., Sladen, A., Audin, L., Farber, D. L., and Soler, P.  
693 Seismic and aseismic slip on the Central Peru megathrust. *Nature*, 465(7294):78–81, 2010. doi: 10.1038/nature09062.
- 694 Peyrat, S. and Favreau, P. Kinematic and spontaneous rupture models of the 2005 Tarapacá intermediate depth earthquake. *Geophysical*  
695 *Journal International*, 181(1):369–381, 2010. doi: 10.1111/j.1365-246X.2009.04493.x.
- 696 Peyrat, S., Campos, J., de Chaballier, J. B., Perez, A., Bonvalot, S., Bouin, M. P., Legrand, D., Nercessian, A., Charade, O., Patau, G., Clévédae,  
697 E., Kausel, E., Bernard, P., and Vilotte, J. P. Tarapacá intermediate-depth earthquake (Mw 7.7, 2005, northern Chile): A slab-pull event  
698 with horizontal fault plane constrained from seismologic and geodetic observations. *Geophysical Research Letters*, 33(22):1–6, 2006.  
699 doi: 10.1029/2006GL027710.
- 700 Pritchard, M. E. and Simons, M. An aseismic slip pulse in northern Chile and along-strike variations in seismogenic behavior. *Journal of*  
701 *Geophysical Research: Solid Earth*, 111(8), 2006. doi: 10.1029/2006JB004258.
- 702 Pritchard, M. E., Norabuena, E. O., Ji, C., Boroschek, R., Comte, D., Simons, M., Dixon, T. H., and Rosen, P. A. Geodetic, teleseismic, and  
703 strong motion constraints on slip from recent southern Peru subduction zone earthquakes. *Journal of Geophysical Research: Solid Earth*,  
704 112(3), 2007. doi: 10.1029/2006JB004294.
- 705 Radiguet, M., Cotton, F., Vergnolle, M., Campillo, M., Walpersdorf, A., Cotte, N., and Kostoglodov, V. Slow slip events and strain accumulation  
706 in the Guerrero gap, Mexico. *Journal of Geophysical Research: Solid Earth*, 117(4), 2012. doi: 10.1029/2011JB008801.
- 707 Radiguet, M., Perfettini, H., Cotte, N., Gualandi, A., Valette, B., Kostoglodov, V., Lhomme, T., Walpersdorf, A., Cabral Cano, E., and Campillo,  
708 M. Triggering of the 2014 Mw7.3 Papanoa earthquake by a slow slip event in Guerrero, Mexico. *Nature Geoscience*, 9(11):829–833, 2016.  
709 doi: 10.1038/ngeo2817.
- 710 Reid, H. F. The Mechanism of the Earthquake. The California Earthquake of April 18, 1906: Rep. of the State Investigation Commiss. Vol. 2.  
711 P. 1. Technical report, Carnegie Institution of Washington, Washington, D. C., 1910.
- 712 Remy, D., Perfettini, H., Cotte, N., Avouac, J. P., Chlieh, M., Bondoux, F., Sladen, A., Tavera, H., and Socquet, A. Postseismic reloading of the  
713 subduction megathrust following the 2007 Pisco, Peru, earthquake. *Journal of Geophysical Research: Solid Earth*, 121(5):3978–3995, 5  
714 2016. doi: 10.1002/2015JB012417.
- 715 Reverso, T., Marsan, D., Helmstetter, A., and Enescu, B. Background seismicity in Boso Peninsula, Japan: Long-term acceleration, and  
716 relationship with slow slip events. *Geophysical Research Letters*, 43(11):5671–5679, 2016. doi: 10.1002/2016GL068524.
- 717 Romanet, P., Bhat, H. S., Jolivet, R., and Madariaga, R. Fast and Slow Slip Events Emerge Due to Fault Geometrical Complexity. *Geophysical*

- 718 *Research Letters*, 45(10):4809–4819, 2018. doi: 10.1029/2018GL077579.
- 719 Rousset, B., Campillo, M., Lasserre, C., Frank, W. B., Cotte, N., Walpersdorf, A., Socquet, A., and Kostoglodov, V. A geodetic matched filter  
720 search for slow slip with application to the Mexico subduction zone. *Journal of Geophysical Research: Solid Earth*, 122(12):498–10, 12  
721 2017. doi: 10.1002/2017JB014448.
- 722 Rousset, B., Bürgmann, R., and Campillo, M. Slow slip events in the roots of the San Andreas fault. *Science Advances*, 5(2):eaav3274, 2 2019.  
723 doi: 10.1126/sciadv.aav3274.
- 724 Ruegg, J. C., Olcay, M., and Lazo, D. Co-, Post- and Pre(?) -seismic Displacements Associated with the Mw 8.4 Southern Peru Earthquake of  
725 23 June 2001 from Continuous GPS Measurements. *Seismological Research Letters*, 72(6):673–678, 11 2001. doi: 10.1785/gssrl.72.6.673.
- 726 Ruiz, S. and Madariaga, R. Historical and recent large megathrust earthquakes in Chile. *Tectonophysics*, 733(September 2017):37–56, 2018.  
727 doi: 10.1016/j.tecto.2018.01.015.
- 728 Ruiz, S., Metois, M., Fuenzalida, A., Ruiz, J., Leyton, F., Grandin, R., Vigny, C., Madariaga, R., and Campos, J. Intense foreshocks and a slow  
729 slip event preceded the 2014 Iquique Mw8.1 earthquake. *Science*, 345(6201):1165–1169, 2014. doi: 10.1126/science.1256074.
- 730 Rüpke, L. H., Morgan, J. P., Hort, M., and Connolly, J. A. Serpentine and the subduction zone water cycle. *Earth and Planetary Science*  
731 *Letters*, 223(1-2):17–34, 2004. doi: 10.1016/j.epsl.2004.04.018.
- 732 Savage, J. C. A dislocation model of strain accumulation and release at a subduction zone. *Journal of Geophysical Research: Solid Earth*, 88  
733 (B6):4984–4996, 6 1983. doi: 10.1029/JB088iB06p04984.
- 734 Schurr, B., Asch, G., Rosenau, M., Wang, R., Oncken, O., Barrientos, S., Salazar, P., and Vilotte, J. P. The 2007 M7.7 Tocopilla northern Chile  
735 earthquake sequence: Implications for along-strike and downdip rupture segmentation and megathrust frictional behavior. *Journal of*  
736 *Geophysical Research: Solid Earth*, 117(5), 2012. doi: 10.1029/2011JB009030.
- 737 Schurr, B., Asch, G., Hainzl, S., Bedford, J., Hoechner, A., Palo, M., Wang, R., Moreno, M., Bartsch, M., Zhang, Y., Oncken, O., Tilmann, F., Dahm,  
738 T., Victor, P., Barrientos, S., and Vilotte, J.-P. Gradual unlocking of plate boundary controlled initiation of the 2014 Iquique earthquake.  
739 *Nature*, 512(7514):299–302, 8 2014. doi: 10.1038/nature13681.
- 740 Schurr, B., Moreno, M., Tréhu, A. M., Bedford, J., Kummerow, J., Li, S., and Oncken, O. Forming a Mogi Doughnut in the Years  
741 Prior to and Immediately Before the 2014 M8.1 Iquique, Northern Chile, Earthquake. *Geophysical Research Letters*, 47(16), 2020.  
742 doi: 10.1029/2020GL088351.
- 743 Shrivastava, M. N., González, G., Moreno, M., Soto, H., Schurr, B., Salazar, P., and Báez, J. C. Earthquake segmentation in northern Chile  
744 correlates with curved plate geometry. *Scientific Reports*, 9(1):4403, 12 2019. doi: 10.1038/s41598-019-40282-6.
- 745 Simons, M., Galetzka, J. E., Genrich, J. F., Ortega, F., Comte, D., Glass, B., Gonzalez, G., and Norabuena, E. Central Andean Tectonic Obser-  
746 vatory Geodetic Array - GPS/GNSS Observations. Technical report, Caltech, 2010.
- 747 Sippl, C., Schurr, B., Asch, G., and Kummerow, J. Seismicity Structure of the Northern Chile Forearc From >100,000 Double-Difference  
748 Relocated Hypocenters\ . *Journal of Geophysical Research: Solid Earth*, 123(5):4063–4087, 2018. doi: 10.1002/2017JB015384.
- 749 Sippl, C., Schurr, B., Münchmeyer, J., Barrientos, S., and Oncken, O. The Northern Chile forearc constrained by 15 years of permanent  
750 seismic monitoring. *Journal of South American Earth Sciences*, 126(December 2022):104326, 6 2023. doi: 10.1016/j.jsames.2023.104326.
- 751 Sladen, A., Tavera, H., Simons, M., Avouac, J. P., Konca, A. O., Perfettini, H., Audin, L., Fielding, E. J., Ortega, F., and Cavagnoud, R. Source  
752 model of the 2007 Mw8.0 Pisco, Peru earthquake: Implications for seismogenic behavior of subduction megathrusts. *Journal of Geo-*  
753 *physical Research: Solid Earth*, 115(2), 2010. doi: 10.1029/2009JB006429.
- 754 Socquet, A., Valdes, J. P., Jara, J., Cotton, F., Walpersdorf, A., Cotte, N., Specht, S., Ortega-Culaciati, F., Carrizo, D., and Norabuena, E. An  
755 8 month slow slip event triggers progressive nucleation of the 2014 Chile megathrust. *Geophysical Research Letters*, 44(9):4046–4053, 5

2017. doi: 10.1002/2017GL073023.
- Steinbrugge, K. V., Zacher, E. G., Tocher, D., Whitten, C. A., and Claire, C. N. Creep on the San Andreas fault. *Bulletin of the Seismological Society of America*, 50(3):389–415, 7 1960.
- Supino, M., Poiata, N., Festa, G., Vilotte, J. P., Satriano, C., and Obara, K. Self-similarity of low-frequency earthquakes. *Scientific Reports*, 10(1):6523, 12 2020. doi: 10.1038/s41598-020-63584-6.
- Takagi, R., Uchida, N., and Obara, K. Along-Strike Variation and Migration of Long-Term Slow Slip Events in the Western Nankai Subduction Zone, Japan. *Journal of Geophysical Research: Solid Earth*, 124(4):3853–3880, 2019. doi: 10.1029/2018JB016738.
- Tarantola, A. *Inverse Problem Theory and Methods for Model Parameter Estimation*. SIAM, 2005. doi: 10.1137/1.9780898717921.
- Tassara, A. and Echaurren, A. Anatomy of the Andean subduction zone: three-dimensional density model upgraded and compared against global-scale models. *Geophysical Journal International*, 189(1):161–168, 4 2012. doi: 10.1111/j.1365-246X.2012.05397.x.
- Teunissen, P. J. and Montenbruck, O., editors. *Springer Handbook of Global Navigation Satellite Systems*. Springer International Publishing, Cham, 2017. doi: 10.1007/978-3-319-42928-1.
- Tissandier, R., Nocquet, J., Klein, E., Vigny, C., Ojeda, J., and Ruiz, S. Afterslip of the M<sub>w</sub> 8.3 2015 Illapel Earthquake Imaged Through a Time-Dependent Inversion of Continuous and Survey GNSS Data. *Journal of Geophysical Research: Solid Earth*, 128(2):1–21, 2 2023. doi: 10.1029/2022JB024778.
- Twardzik, C., Duputel, Z., Jolivet, R., Klein, E., and Rebischung, P. Bayesian inference on the initiation phase of the 2014 Iquique, Chile, earthquake. *Earth and Planetary Science Letters*, 600:117835, 2022. doi: 10.1016/j.epsl.2022.117835.
- Uchida, N., Takagi, R., Asano, Y., and Obara, K. Migration of shallow and deep slow earthquakes toward the locked segment of the Nankai megathrust. *Earth and Planetary Science Letters*, 531:115986, 2020. doi: 10.1016/j.epsl.2019.115986.
- van Rijnsingen, E. M., Calais, E., Jolivet, R., de Chabalier, J., Jara, J., Symithe, S., Robertson, R., and Ryan, G. A. Inferring Interseismic Coupling Along the Lesser Antilles Arc: A Bayesian Approach. *Journal of Geophysical Research: Solid Earth*, 126(2):1–21, 2 2021. doi: 10.1029/2020JB020677.
- Vigny, C. and Klein, E. The 1877 megathrust earthquake of North Chile two times smaller than thought? A review of ancient articles. *Journal of South American Earth Sciences*, 117:103878, 8 2022. doi: 10.1016/j.jsames.2022.103878.
- Villegas-Lanza, J. C., Chlieh, M., Cavalié, O., Tavera, H., Baby, P., Chire-Chira, J., and Nocquet, J.-M. Active tectonics of Peru: Heterogeneous interseismic coupling along the Nazca megathrust, rigid motion of the Peruvian Sliver, and Subandean shortening accommodation. *Journal of Geophysical Research: Solid Earth*, 121(10):7371–7394, 10 2016. doi: 10.1002/2016JB013080.
- Voss, N., Dixon, T. H., Liu, Z., Malservisi, R., Protti, M., and Schwartz, S. Do slow slip events trigger large and great megathrust earthquakes? *Science advances*, 4(10):eaat8472, 10 2018. doi: 10.1126/sciadv.aat8472.
- Wallace, L. M. Slow Slip Events in New Zealand. *Annual Review of Earth and Planetary Sciences*, 48(1):175–203, 5 2020. doi: 10.1146/annurev-earth-071719-055104.
- Wang, H., Huismans, R. S., and Rondenay, S. Water Migration in the Subduction Mantle Wedge: A Two-Phase Flow Approach. *Journal of Geophysical Research: Solid Earth*, 124(8):9208–9225, 2019. doi: 10.1029/2018JB017097.
- Williams, S. D. P. The effect of coloured noise on the uncertainties of rates estimated from geodetic time series. *Journal of Geodesy*, 76(9-10):483–494, 2003. doi: 10.1007/s00190-002-0283-4.
- Zhu, L. and Rivera, L. A. A note on the dynamic and static displacements from a point source in multilayered media. *Geophysical Journal International*, 148(3):619–627, 3 2002. doi: 10.1046/j.1365-246X.2002.01610.x.

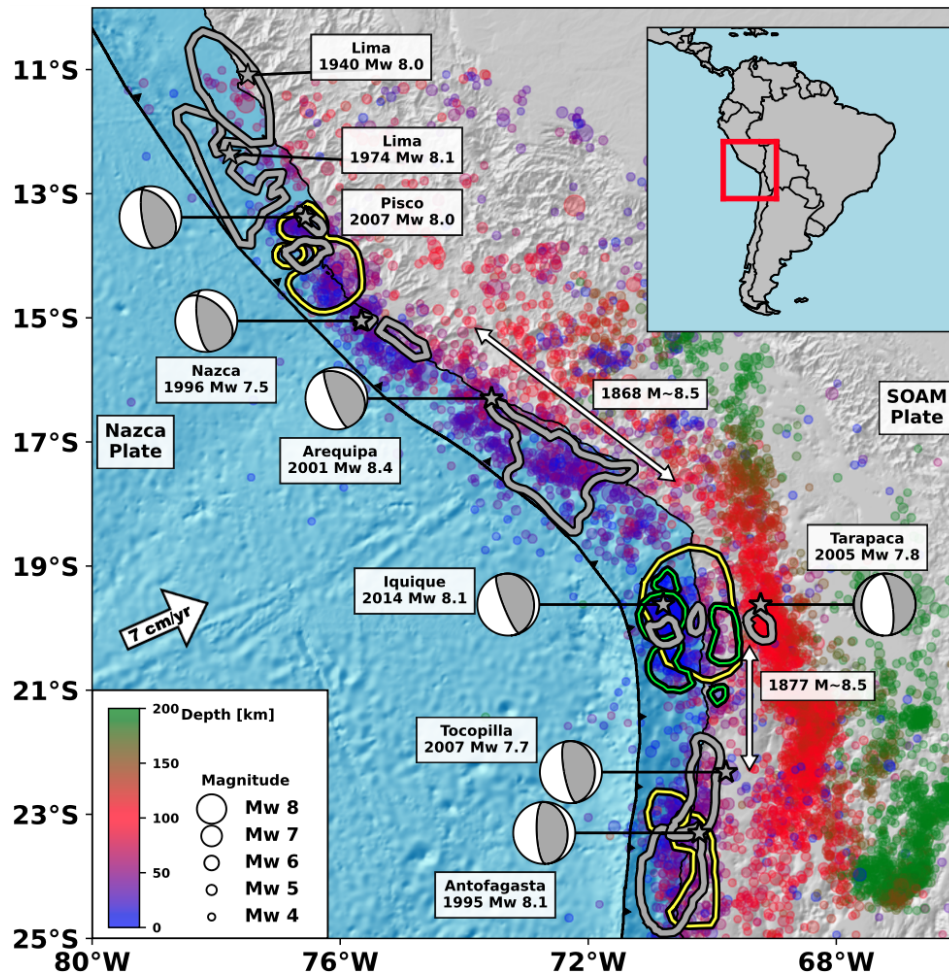


**Figure 1** Seismotectonic map of the South Peru - North Chile subduction zone. White arrows show the extent of historical earthquakes (Comte and Pardo, 1991; Vigny and Klein, 2022). Gray contours are the rupture area of instrumental earthquakes with  $M > 7.5$ , with corresponding epicenters (gray stars) and focal mechanisms (if available) (Dorbath et al., 1990; Beck and Ruff, 1989; Hartzell and Langer, 1993; Delouis et al., 1997; Chlieh et al., 2004; Pritchard et al., 2007; Dziewonski et al., 1981; Ekström et al., 2012; Peyrat and Favreau, 2010; Sladen et al., 2010; Béjar-Pizarro et al., 2010; Duputel et al., 2015; Jara et al., 2018). Yellow lines are the 0.1 m afterslip contours available in the region (Chlieh et al., 2004; Béjar-Pizarro et al., 2010; Remy et al., 2016; Hoffmann et al., 2018), whereas the green ones are the pre-seismic slip reported for Iquique earthquake by Socquet et al. (2017). Color-coded dots indicate seismicity with  $M > 4.0$  from the International Seismological Centre (International Seismological Centre, 2016) over the period 1990 - 2016, color-coded by depth and scaled by magnitude. Large white arrow shows convergence direction and rate from Métouis et al. (2016). SOAM: South America plate.



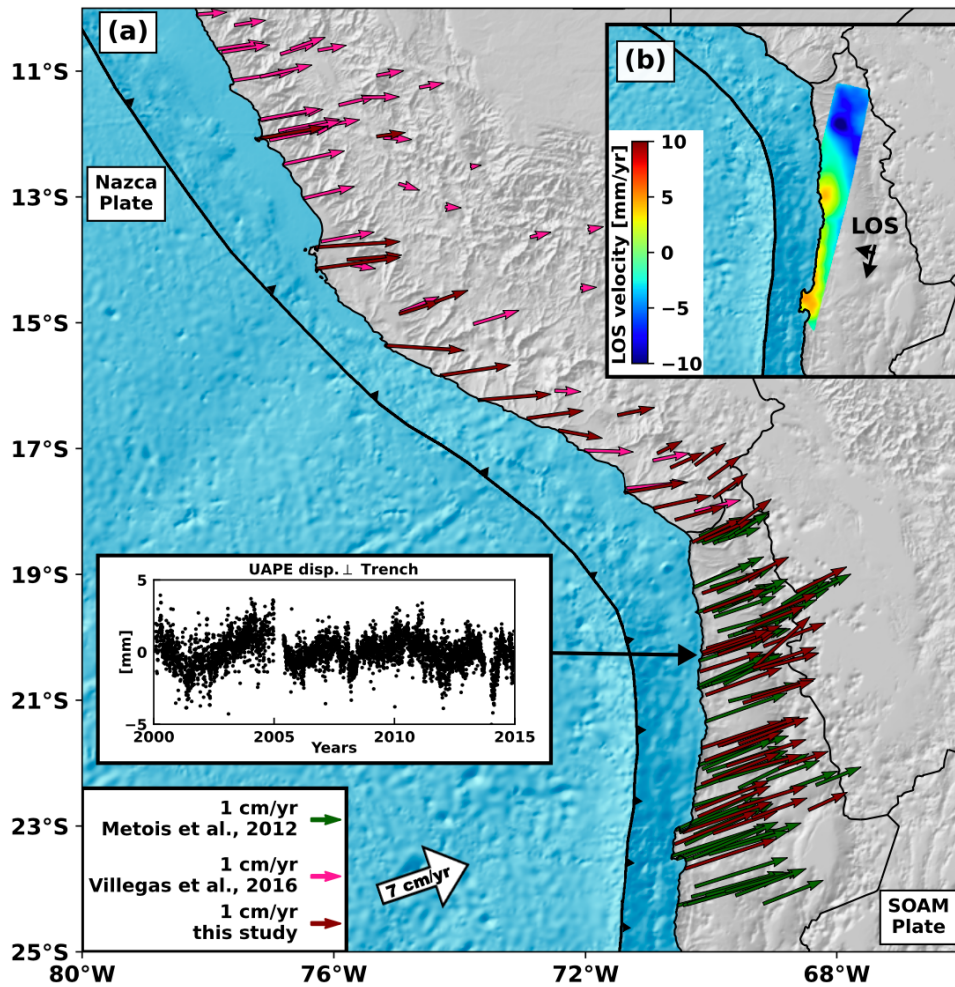


**Figure 2** Geodetic data. (a) Colored dark green and pink arrows are the GNSS interseismic velocities from Métois et al. (2016) and Villegas-Lanza et al. (2016), respectively, while brown arrows are the continuous GNSS processed in this study. The inset shows the residual trench perpendicular displacement for GNSS station UAPE. (b) Line-of-sight (LOS) interseismic ground velocity from track 96 (Envisat data) from (Jolivet and Simons, 2018; Jolivet et al., 2020). Black arrows indicate the flight direction of the satellite and its line of sight (LOS).

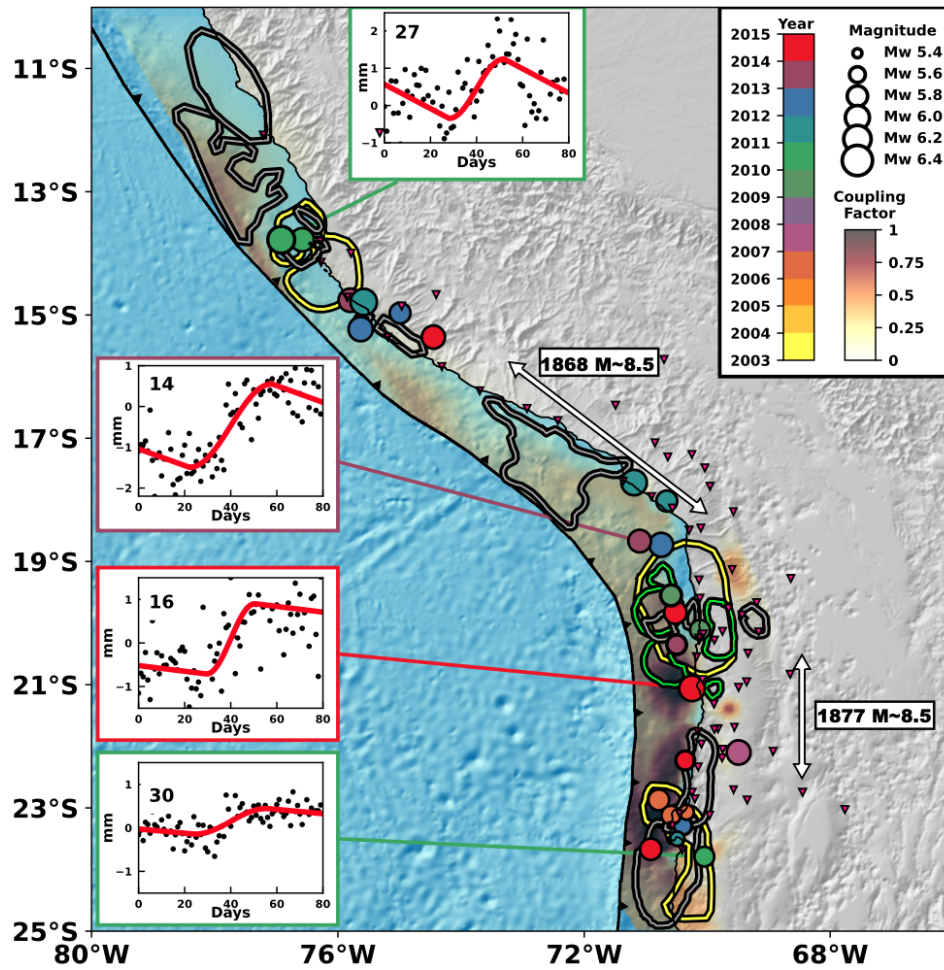


**Figure 3** Location of detected aseismic slip events. Markers are color-coded by time of occurrence and scaled by magnitude. Four examples of weighted stacked correlations are shown with the event id number. Red line is the best fit model used to evaluate the event magnitude and duration. Background color from white to dark through yellow and red is the mean coupling distribution. Black red areas ( $C \sim 1$ ) are locked regions, while transparent areas ( $C \sim 0$ ) are regions that slip aseismically at a rate equal to the plate convergence rate. Gray contours are instrumental rupture areas. Yellow contours are afterslip regions, whereas green ones are Iquique earthquake preseismic slip. As indicated in Figure 1, white arrows are the historical rupture extensions.



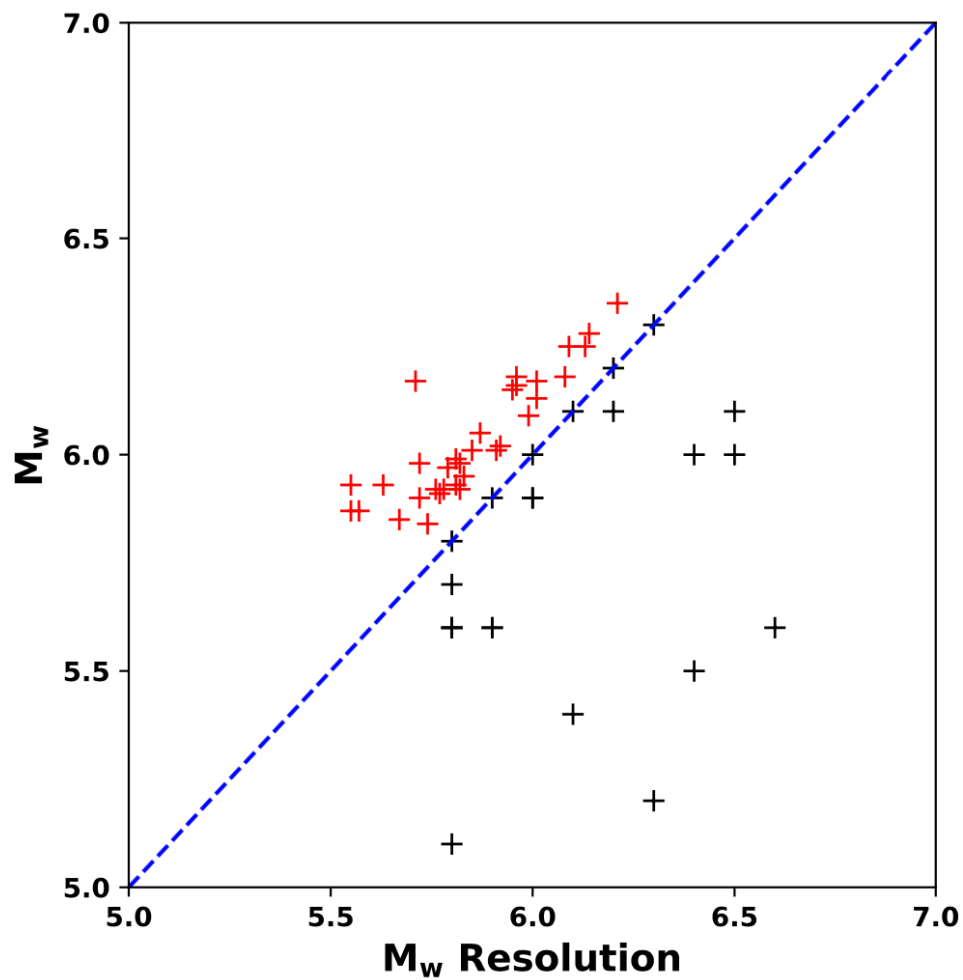


**Figure 4** Event magnitude as a function of the resolution magnitude of the node where the event is located. Red crosses are events that passed the resolution test. Dashed blue line is the identity that separates validated from excluded events.

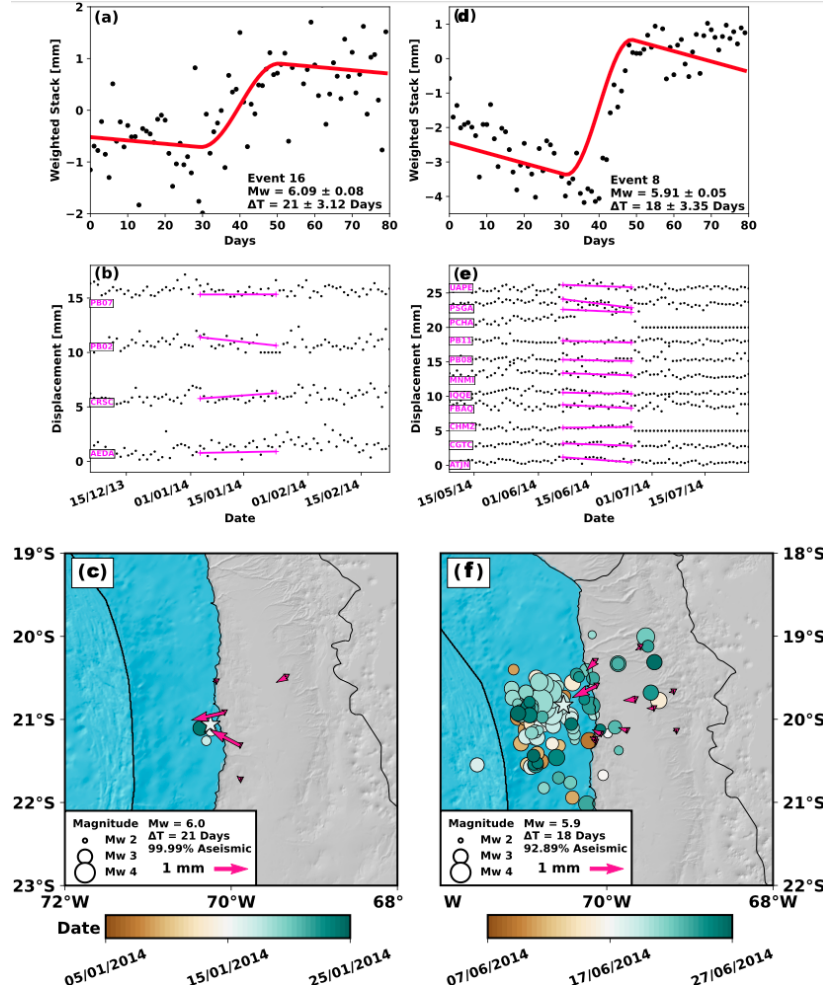


**Figure 5** Examples of detected aseismic slip events in the vicinity of the 2014 Iquique earthquake, their locations, and associated seismicity. (a) and (d), weighted stacks for events #16 #and 8. Red line is the preferred model used to estimate duration and magnitude, indicated at the bottom right of each plot. Amplitude of horizontal displacement time series (b and e,  $\sqrt{N_{disp}^2 + E_{disp}^2}$ ) for stations used to compute the weighted stack on (a) and (c). Pink is the static displacement used to characterize the different event parameters (magnitude and duration). (c) and (f) are events' locations denoted by white stars. Dots are seismicity occurring before and after the event (half of the event duration for each period), scaled by magnitude and color-coded by date. Inverted triangles are the GNSS station locations. Pink arrows are the GNSS displacement during the detected slow slip event.

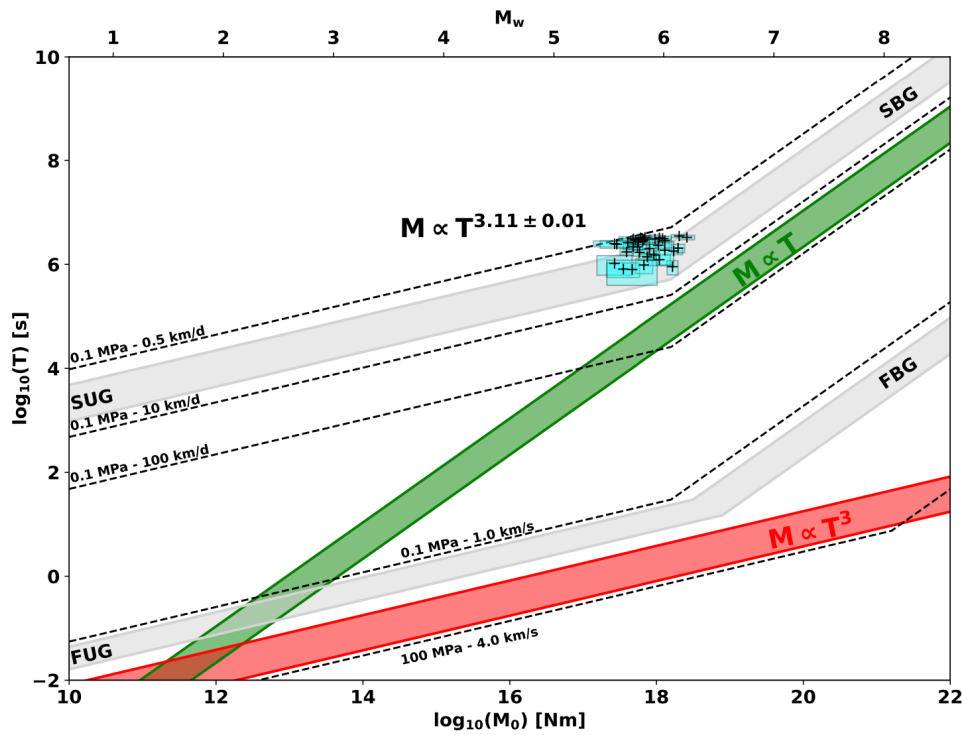


**Figure 6** Seismic moment versus duration for our aseismic slip events following the scaling law proposed by [Gomberg et al. \(2016\)](#). Slow bounded/unbounded (SBG, SUG) and fast bounded/unbounded (FBG, FUG) regions are shown by light gray areas. Dashed lines are the theoretical relationship between moment and duration for a few selected stress-drop and rupture velocity values. The  $M \propto T$  scaling is shown in green. The  $M \propto T^3$  scaling is shown in red.

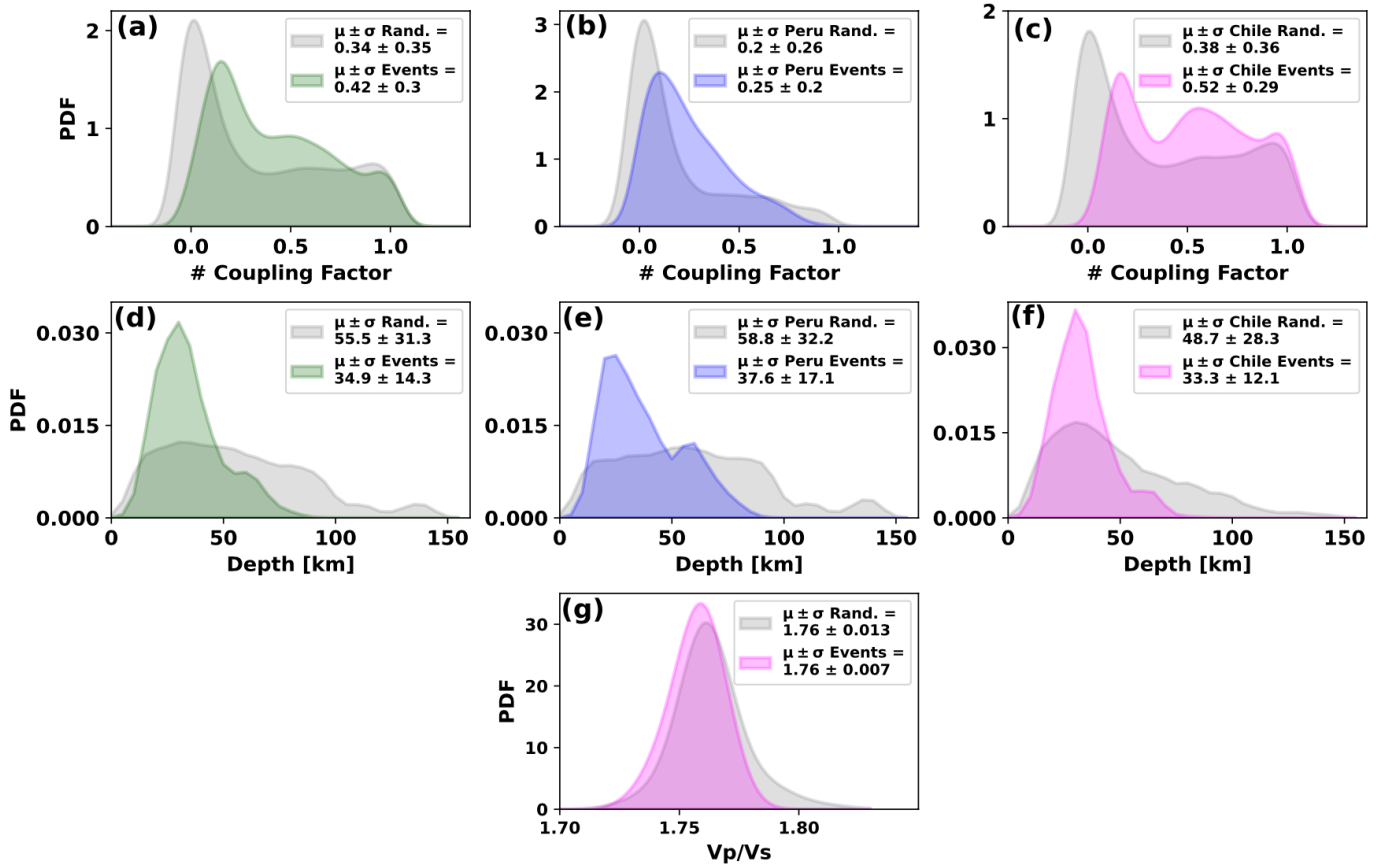


**Figure 7** Coupling, depth, and Vp/Vs ratio of the detected aseismic slip events. (a) Probability Density Functions (PDF) of 1000 coupling models for 33 random picks (gray) and PDF of coupling where 33 aseismic slip events are detected (green), with respective mean ( $\mu$ ) and standard deviations ( $\sigma$ ). (b) and (c) are the same as (a) for the Peru region only (gray: random, blue: SSEs) and northern Chile only (gray: random, magenta: events), respectively. (d) PDF of the depths of 33 random events (gray) and aseismic slip events detected in the region (green). (e) and (f) Same as (d) but for Peru (gray: random, blue: events) and Chile (gray, magenta) regions. (g) PDF of the Vp/Vs ratio for the Chilean region (gray, 33 random events), and detected aseismic events in Chile (magenta).

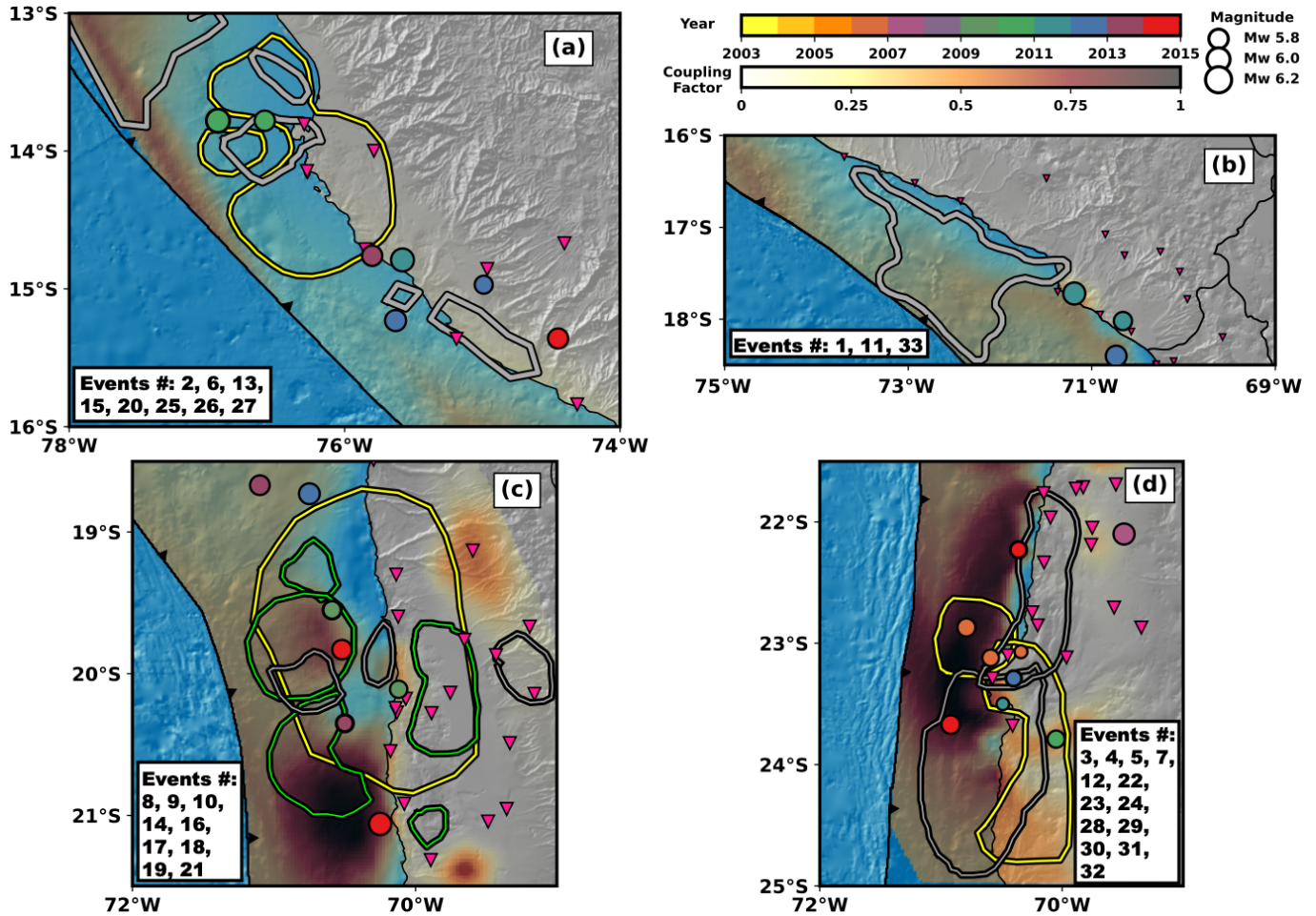


**Figure 8** Zoom by region of Seismic/Aseismic information. Gray contours are instrumental ruptures, whereas yellow ones relate to reported afterslip. Our aseismic slip events are color-coded by time and scaled by magnitude. In the background, our Bayesian inference of coupling. Inverted pink triangles are the GNSS stations used in this study. (a) Region struck by the Nazca (1996) and Arequipa (2007) earthquakes. Our detections seem to cluster around asperities broken during earthquakes or afterslip regions. (b) Region struck by the Arequipa (2001) earthquake. (d) Region struck by the Iquique earthquake in 2014. Green contours denote the aseismic slip events reported by [Socquet et al. \(2017\)](#). Events occur around locked interseismic patches or low-coupled regions. (d) Region struck by the Antofagasta (1995) and Tocopilla (2007) earthquakes. Events surround broken asperities or locked interseismic patches, with a cluster beneath Mejillones Peninsula, potentially associated with earthquake afterslip. For citations of instrumental ruptures and afterslip, please refer to Figure 1

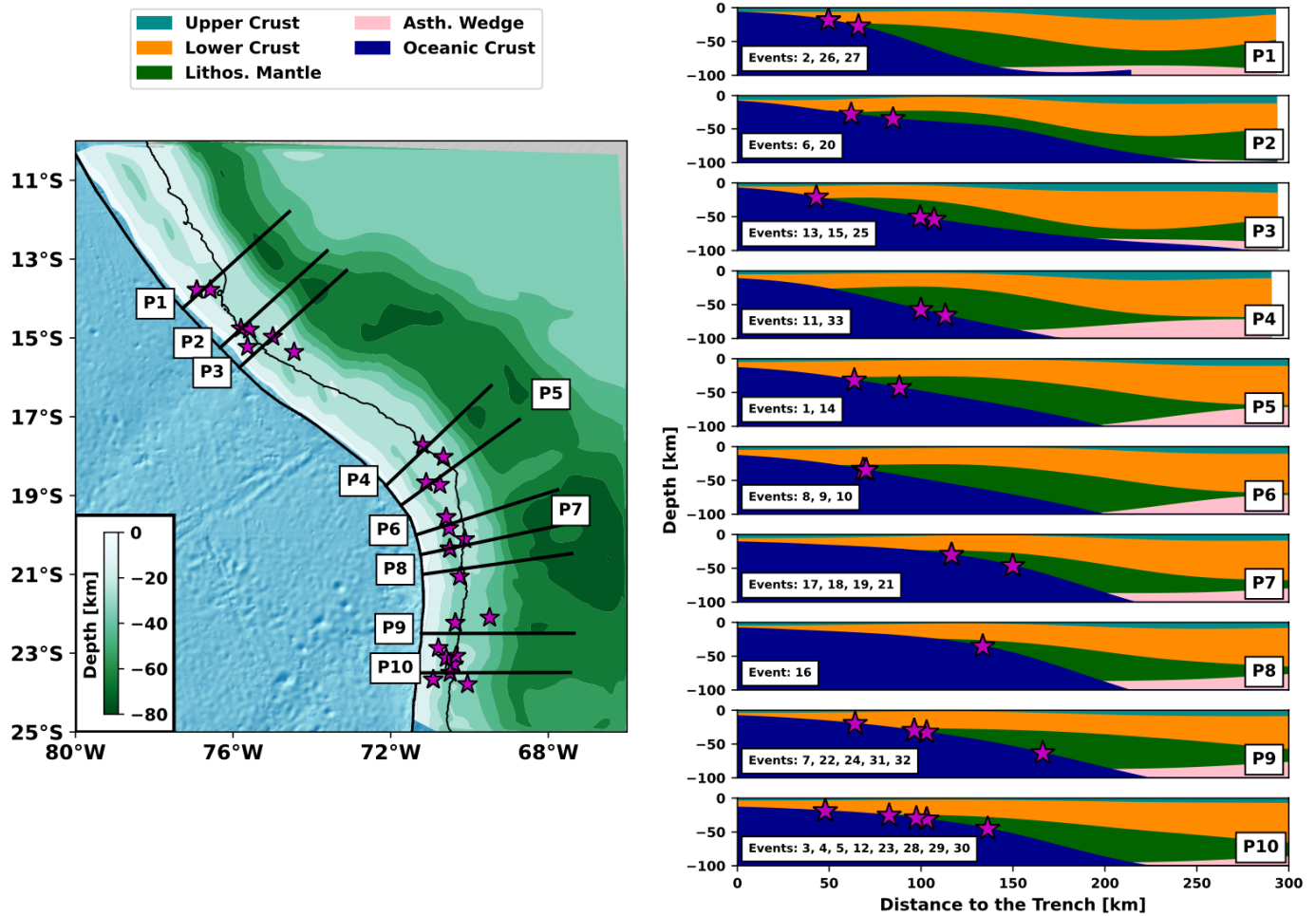


**Figure 9** Map view of the depth of the continental Moho discontinuity, extracted from gravimetric models by [Tassara and Echaurren \(2012\)](#). Magenta stars are the location of 33 aseismic events, while black lines indicate the location of the profiles shown on the right. Colors indicate the structure at depth (upper and lower crusts, lithospheric mantle, asthenospheric wedge, and oceanic crust). White box indicates the id of events occurring along each profile.